UNIVERSITY OF LEEDS

This is a repository copy of *Affimer Tagged Cubosomes: Targeting of Carcinoembryonic Antigen Expressing Colorectal Cancer Cells Using In Vitro and In Vivo Models*.

White Rose Research Online URL for this paper:
https://eprints.whiterose.ac.uk/184492/

Version: Accepted Version

Article:

White Rose
university consortium
Universities of Leeds, Sheffield & York

eprints@whiterose.ac.uk
https://eprints.whiterose.ac.uk/

1   # Affimer Tagged Cubosomes: Targeting of

2   # Carcinoembryonic Antigen Expressing Colorectal

3   # Cancer Cells using *In Vitro and In Vivo* Models

4   *Arindam Pramanik[1,2*], Zexi Xu[3,4], Shazana H. Shamsuddin[1,5], Yazan S. Khaled[2], Nicola Ingram[6],*

5   *Thomas Maisey[2], Darren Tomlinson[7],P. Louise Coletta[6], David Jayne[6], Thomas A. Hughes[2*],*

6   *Arwen I.I. Tyler[3*] and Paul A. Millner[1*]*

7   [1]School of Biomedical Sciences, University of Leeds, Leeds, LS2 9JT, United Kingdom

8   [2]School of Medicine, University of Leeds, Leeds, LS9 7TF, United Kingdom

9   [3]School of Food Science and Nutrition, University of Leeds, Leeds, LS2 9JT, United Kingdom

10   [4]School of Chemistry and Astbury Centre for Structural Molecular Biology, University of Leeds,
11   Leeds, LS2 9JT, United Kingdom

12   [5]Department of Pathology, School of Medical Sciences, Universiti Sains Malaysia, 16150,
13   Malaysia

14   [6]Leeds Institute of Medical Research, St James's University Hospital, Leeds, LS9 7TF United
15   Kingdom

16   [7]Biomedical Health Research Centre, BioScreening Technology Group, University of Leeds,
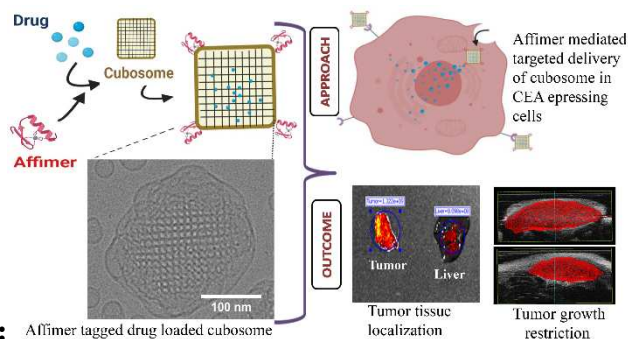17   Leeds, LS2 9JT, United Kingdom

18

19

20

TOC: Affimer tagged drug loaded cubosome

ABSTRACT

Nanomedicines, while having been approved for cancer therapy, present many challenges such as low stability, rapid clearance and non-specificity leading to off-target toxicity. Cubosomes are porous lyotropic liquid crystalline nanoparticles that have shown great premise as drug delivery vehicles, however their behavior *in vivo* is largely underexplored, hindering clinical translation. Here, we have engineered cubosomes based on space group Im3m, that are loaded with copper acetylacetonate as a model drug and their surface functionalized for the first time with Affimer proteins via copper-free click chemistry to actively target overexpressed carcinoembryonic antigens on LS174T colorectal cancer cells. Unlike non-targeted cubosomes, Affimer tagged cubosomes showed preferential accumulation in cancer cells compared to normal cells not only *in vitro* (2D monolayer cell culture and 3D spheroid models) but also *in vivo* in colorectal cancer mouse xenografts, whilst exhibiting low non-specific absorption and toxicity in other vital organs. Cancerous spheroids had maximum cell death compared to non-cancerous cells upon targeted

39   delivery. Xenografts subjected to targeted drug-loaded cubosomes showed a 5-7 fold higher drug

40   accumulation in the tumor tissue compared to the liver, kidneys and other vital organs, significant

41   decrease in tumor growth and an increased survival rate compared to the non-targeted group. This

42   work encompasses the first thorough pre-clinical investigation of Affimer targeted cubosomes as

43   a cancer therapeutic.

44

45   **INTRODUCTION**

46   Nanomedicine is an emerging field that has shown great potential in providing state of the art

47   diagnosis and treatment of many diseases and a plethora of nanoparticle formulations have been

48   developed based on proteins, polymers, lipids, metals or inorganic elements.[1] An emerging class

49   of lipid-based nanoparticles are dispersions of inverse lyotropic liquid crystalline phases. These

50   have internal nanostructures that possess two- or three-dimensional periodicity, such as hexagonal

51   or cubic symmetries, and are usually stabilized by a polymer corona.   These lyotropic liquid

52   crystalline lipid nanoparticles (LCNPs) offer several advantages such as structural versatility,

53   porosity, improved stability, high encapsulation efficiency due to their high internal surface area,

54   as well as biocompatibility due to mostly being made up of food-grade material.[2-3] Cubosomes, a

55   type of LCNPs, have attracted interest as delivery vectors for theranostic applications. They have

56   an internal structure based on either the diamond, primitive or gyroid bicontinuous cubic phases

57   belonging to space groups Pn3m, Im3m and Ia3d respectively, and consist of two non-

58   communicating water channels divided by a single continuous lipid bilayer (**Figure 1**).[2-3]

59   Cubosomes have potential to offer controlled release of encapsulated actives [4-6] that can also be

60   achieved via phase transitions in response to a stimulus such as pH[7-8] as well as facilitated cellular

61   uptake.[9-10] Due to their amphiphilic nature, they can encapsulate hydrophilic and hydrophilic cargo[2]

62   including drugs, imaging agents,[11] and biomolecular payloads such as proteins[12], DNA[13] or small

63   interfering RNA.[14] LCNPs have been reported to have superior performance and efficacy of the

64   loaded cargo in a variety of disease sites and models.[3] For example, cubosomes outperformed

65   liposomes in siRNA delivery and transfection.[14]

66   Whilst many anti-cancer drugs have been encapsulated into cubosomes and tested for efficacy

67   in a number of different cell lines to mimic various disease models with promising results[15-17], these

68   have mostly been based on passive targeting of nanoparticles, which often requires high drug

69   loading that can lead to off-target toxicity. Cubosomes made entirely of polymers have also been

70   recently synthesized,[18-19] although to the best of our knowledge there have been no studies on the

71   encapsulation of actives within them or their use in biomedical applications. While polymer

72   nanoparticles offer advantages such as increased stability compared to their lipid counterparts, they

73   also suffer from disadvantages such as low biocompatibility and increased cytotoxicity compared

74   to their lipidic counterparts. A small number of studies have functionalized the outer corona of

75   lipid-based cubosomes with molecules such as biotin[20], folate [21] and epidermal growth factor

76   receptor antibody fragments [22], which showed high affinity and specificity to their target. Alcaraz

77   *et al*. developed cubosomes that could undergo copper-free click chemistry that have the potential

78   to target cell surfaces by metabolic labelling.[23]. Moreover, investigation of cubosome-cell

79   interactions has been limited to 2D monolayer cultures. Recently *Zhai et al*. explored the

80   interaction of paclitaxel-loaded cubosomes with 3D spheroid models of skin cancer cells, which

81   provides a much more relevant *in vitro* model to mimic *in vivo* conditions, and found that cancer

82   cells in the spheroids were more resistant to treatment compared to 2D models.[9]

83   Very few studies have focused on the cytotoxicity and, in particular, the biodistribution of

84   cubosomes *in vivo* [3, 9, 11, 22, 24] and as all these studies have had different theranostic applications,

85   used different administration routes and varied compositions of lipids and stabilizer, it is difficult

86   to draw conclusions on the biological fate of cubosomes. For example, Biffi *et al*., showed that

87   fluorescent monoolein cubosomes administered intravenously to the tail vein of healthy mice

88   preferentially accumulated in the liver as monitored over time and up to 48 hours post injection.[25]

89   On the contrary, intraperitoneal injection of paclitaxel-loaded monoolein cubosomes to A431 skin

90   cancer mouse xenografts showed preferential accumulation at tumor sites, monitored up to 24

91   hours post injection.[9]

92   In this work, we aim to develop active cancer-targeted cubosomes to colorectal cancer cells

93   loaded with a model anticancer drug and investigate their efficacy both *in vivo* and *in vitro*, and

94   their efficacy and biodistribution *in vivo* – the first study to perform such a thorough pre-clinical

95   investigation. The heterogeneity between individual colorectal cancers (CRC) and the lack of

96   consistently overexpressed receptors that can be used as biomarkers limit targeted drug delivery.[26]

97   We have previously shown that the most suitable surface biomarker in CRC, both in terms of

98   degree and frequency of overexpression, is a carcinoembryonic antigen (CEA). [27] CEA has been

99   used as a biomarker to image CRC *in vivo*, using fluorescent silica nanoparticles tagged with

100   monoclonal antibodies (mAb).[28] Bottlenecks associated with mAb based drug conjugates however

101   include high cost of production, stability, and batch-to-batch variation, which limit their clinical

102   development. [29-30] Affimers are small proteins that are engineered to have similar binding and

103   specificity as mAbs but offer advantages such as increased stability over a range of conditions

104   (temperature, pH) and ease of production/scale up thereby ensuring consistency over batch-to-

105   batch productions, while maintaining specific target recognition.[31-34] Affimers, identified from a

106   phage display library, that have specificity towards CEA antigens have been developed [35] and

107   exhibit ease of surface functionalization on molecules of interest. [36]

108   Here we have developed monoolein (MO) based cubosomes (Figure 1) that encapsulated with 5

109   weight % (with respect to MO) of the model organometallic cancer drug copper acetylacetonate

110   (CuAc). We were specifically interested in relatively simple copper compounds as anti-cancer

111   agents as they have potential to provide novel and low-cost drugs that could be affordable in a

112   global context.[37] We have previously shown that CuAc has potent anticancer activity however due

113   to its poor solubility and cytotoxicity an encapsulation strategy is necessary.[38-39] The CuAc loaded

114   cubosomes were targeted to CRC cells using Affimers, attached on the cubosome's surface via

115   copper-free click chemistry. Cubosomes were characterized using Small Angle X-ray Scattering

116   (SAXS), cryogenic Transmission Electron Microscopy (cryo-TEM) and dynamic light scattering

117   (DLS). The therapeutic efficacy of the nanoformulation was studied both *in vitro* in CRC 2D

118   monolayer cultures and 3D spheroids as well as tumor xenograft bearing mice, and showed

119   selectivity towards CEA expressing cells. Cancerous spheroids showed maximum cell death

120   compared to non-cancerous cells upon targeted delivery and CRC xenografts showed a large

121   decrease in tumor volume, no off-target toxicity and increased survival rates. The localization of

122   the cubosomes both *in vitro* and *in vivo* was also studied using fluorescence tags and show

123   preferential uptake of the targeted cubosomes by cancerous CEA expressing cells.

124

125
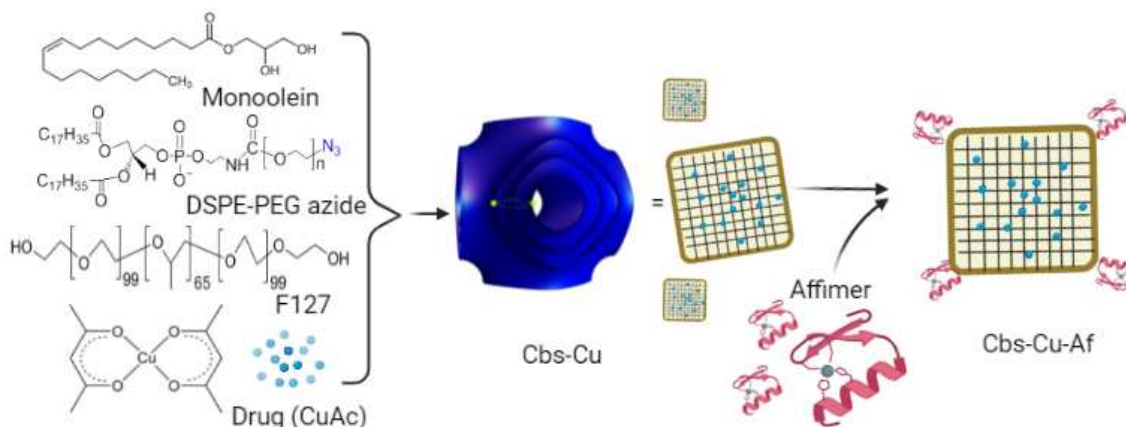
Figure 1: Monoolein based dispersions of the primitive inverse bicontinuous cubic phase (cubosomes, shown in blue), which is based on space group Im3m, were engineered to encapsulate the model organometallic drug copper acetylacetonate (CuAc). The nanoparticles were stabilized by Pluronic F127 and DSPE-PEG2000-azide. DSPE-PEG2000-azide in the outer corona allowed conjugation of Affimer proteins, engineered to have a DCBO functional group, to the cubosome via copper free click chemistry in order to target overexpressed carcinoembryonic antigens on colorectal cancer cells.

RESULTS AND DISCUSSION

Characterization of clickable cubosomes tagged with Affimer protein

We formulated and characterized monoolein (MO) based cubosomes stabilized by Pluronic F127, and DSPE-PEG2000-azide and loaded with a model hydrophobic drug. DSPE-PEG2000-azide, apart from acting as a stabilizer, has the additional role of allowing surface functionalization of the cubosomes with any ligand with dibenzocyclooctyne (DBCO) groups via copper free click chemistry. Appreciating that size might be an important consideration when designing nanocarriers,[40-42] as larger particles (>200nm) may potentially limit their ability to reach the tumor tissue whereas smaller particles (<20 nm) have low retention in the tumor and fast clearance *in vivo* [43], we explored different MO:F127:DSPE-PEG ratios and their effect on particle size (**Table S1**).Preliminary exploration of dispersion conditions found that dispersing the particles in an ice

7

145   bath gave smaller particles sizes on average compared to dispersing at room temperature. Out of

146   the compositions tested, MO: DPA: F127 88.79: 4.67: 6.54(w/w) yielded the smallest Z-average

147   diameter of 106 nm as well as the lowest polydispersity index (PDI) of 0.18, and hence this

148   concentration of MO: DPA: F127 was taken forward for all subsequent experiments. It should be

149   noted that the hydrodynamic diameter of the cubosomes as measured by Dynamic Light Scattering

150   (DLS) is not the same as their physical size. The mean size of the nanoparticles obtained from

151   various techniques weighs the size distribution differently so for example, DLS data will

152   emphasize larger particles whereas cryo-TEM often excludes larger particles from the thin ice and

153   hence highlights smaller particles in these polydisperse samples (see comparisons later).

154   Complexes of platinum, ruthenium, titanium and gallium have successfully entered clinical trials,

155   leaving potential for other complexes to be researched as cancer therapeutics[44]. We have used one

156   such metal–organic complex of copper, copper acetylacetonate (CuAc), as a model hydrophobic

157   drug in this study. This complex has been extensively studied in various cancer cells in our

158   previous reports[38-39]. In this study, we found that encapsulating 5% (w/w with respect to MO) of

159   CuAc in cubosomes (Cbs) to be optimum, ensuring stable dispersions for up to 21 days (**Table S2**

160   and hence this loading was used in subsequent studies. The encapsulation of CuAc in the cubosome

161   was confirmed by energy-dispersive X-ray spectroscopy (EDAX). As shown **Figure S1A** and

162   **S1B**, a distinct peak for Cu was noted as expected at 8 KeV, which was not present in the analysis

163   of cubosomes without CuAc. Inductively coupled plasma optical emission spectrometry (ICP-

164   OES) using Cu as a reference material could further evaluate the encapsulation efficiency of CuAc

165   in the cubosome (**Table S2**). Similar to Bazylińska *et al*. [45], where a high encapsulation efficiency

166   was noted for a photosensitizer (Ce6) loaded cubosome, the encapsulation efficiency of 5 wt%

167   CuAc (with respect to MO) in our study was found to be 82% ± 4.0 (**Table S2**). DBCO labeled

168   Affimers were conjugated to the Cbs-Cu (CuAc loaded cubosome) via copper free click chemistry.

169   As shown by the FT-IR spectra (**Figure S1C**), a peak at 2127 cm^{-1} is observed for Cbs-Cu, which

170   signifies the presence of an azide group. The peak disappears for Affimer tagged Cbs-Cu (Cbs-

171   Cu-Af) due to the covalent bonding of the DBCO labelled Affimer to the azide group of DSPE-

172   PEG in the cubosome. Affimer conjugation is further confirmed using EDAX data (**Figure S1B**)

173   which show the characteristic Sulphur Kα and Kβ peaks (2.3 – 2.5 eV) arising from the tagged

174   cubosomes that is due to cysteine present in the Affimer. These peaks are absent in the bare

175   cubosomes (**Figure S1A**). The Cbs-Cu-Af cubosomes showed a prolonged and sustained release

176   of CuAc from the nanoparticles which was up to 60% of its total encapsulation even after 48h

177   (**Figure S1D**).

178   The internal nanostructure of the bare (Cbs), drug loaded (Cbs-Cu) and drug and Affimer tagged

179   (Cbs-Cu-Af) cubosomes was studied by small-angle X-ray scattering (SAXS) at 25ºC and 37ºC

180   (**Figure 2A** and **2B**). The choice of 25ºC justified storage at room temperature and long term

181   stability, whereas 37ºC justified its stability at a physiological relevant temperature. All SAXS

182   patterns show Bragg peaks in the ratio of $\sqrt{2}:\sqrt{4}:\sqrt{6}$ (which correspond to Miller indices (hkl) 110,

183   200, 211) which index as a primitive bicontinuous cubic space belonging to space group Im3m.

184   The lattice parameters of Cbs, Cbs-Cu and Cbs-Cu-Af cubosomes at 25ºC were 144.9 Å, 149.3 Å

185   and 153.8 Å, and 133.3 Å, 135.1 Å and 138.9 Å at 37 ºC respectively. MO is known to form a

186   bicontinuous cubic phase of space group Pn3m in excess water at the temperature range explored

187   in this study, [46-47] however when Pluronic F127 is used to stabilize dispersions of MO, the system

188   transforms to an Im3m phase [48]. Our results, as well as the lattice parameters obtained here are

189   consistent with previous studies on bare cubosomes [9, 23]. Encapsulated 5 wt% CuAc does not cause

190   a phase transition but slightly increases the lattice parameter as the bulky metal complex decreases

191   the magnitude of the monolayer spontaneous inverse curvature. Similarly, addition of DPA causes

192   a further increase in the lattice parameter as it decreases the hydrocarbon chain splay resulting in

193   less curved structures as was previously shown in phytantriol-based cubosomes[23]. The Z-average

194   sizes of Cbs, Cbs-Cu and Cbs-Cu-Af cubosomes at 25ºC were 106, 121 and 141 nm and had a

195   polydispersity index of 0.155, 0.159 and 0.086 respectively (**Figure 2C and S2**). It should be noted

196   that although DLS data on phytantriol: DPA cubosomes showed a bimodal distribution and a

197   significantly larger average size and PDI [23], this was not the case for our MO-based cubosomes.

198   The mean size of Cbs-Cu-Af cubosomes was also calculated by nanoparticle size analysis from

199   cryo-TEM data and gave a mean size of 130nm (**Figure S3A**). This is comparable to the value of

200   141 nm obtained by DLS. TEM nanoparticle size analysis of Cbs-Cu-Af gave a mean size of 66

201   nm (**Figure S3B**) although care should be taken when interpreting this number as TEM

202   measurements of soft materials can lead to deformation and mass loss of the sample.

203

204   The shape and morphology of Cbs-Cu-Af cubosomes was visualized by transmission electron

205   microscopy (TEM) (**Figure 2D**), which showed a neat cubical structure. Their internal

206   nanostructure was further visualized by cryo-TEM (**Figure 2E**). Cryo-TEM images show ordered

207   internal nanostructures which index to space group Im3m (**Figure 2E inset**). Cryo-TEM images

208   show Im3m cubosomes with a small number of vesicular structures which is known and caused

209   due to a surplus of F127 [49].

210

211

212
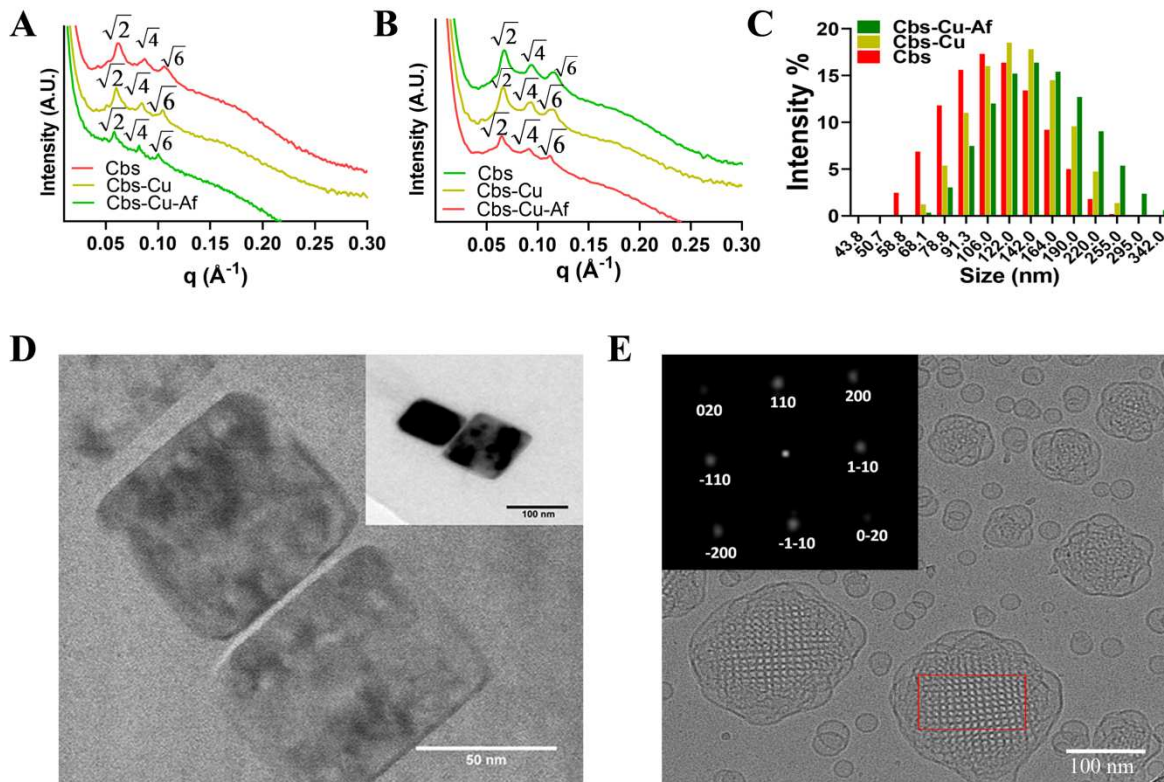
Figure 2: Cubosome characterization. SAXS patterns of Cbs, Cbs-Cu and Cbs-Cu-Af at (A) 25 °C and (B) 37°C. All SAXS patterns index to a primitive bicontinuous cubic phase belonging to space group Im3m. (C) DLS data showing the hydrodynamic diameter of Cbs, Cbs-Cu and Cbs-Cu-Af with a z-average size of 106, 121 and 141nm respectively. (D) TEM image Cbs-Cu-Af and (E) Representative cryo-TEM image of Cbs-Cu-Af. The corresponding intensity of the fast Fourier transform (FFT) applied to the cubosome (red box) is shown in the inset along with the assigned Miller indices which index to space group Im3m.

Carcinoembryonic antigen is a suitable marker for colorectal cancers

Carcinoembryonic antigen (CEA) has been reported as a marker on the surface of cancer cells including lung, breast and pancreatic, yet predominantly its expression has been noted in colon and rectum cancers, as found from clinical samples [50-52]. We have previously reported LoVo CRC cell lines having a relatively high expression of CEA[35]. In this study, we show LS174T CRC cell lines exhibiting high CEA expression compared to non-cancerous HEK-293 cells, using CEA mAb

229   tagged with Alexa Fluor 488 secondary antibody (**Figure S5A**). This was further validated using

230   a western blot from both LS174T and HEK-293 cell lysates (**Figure S5B**), where the expression

231   of CEA was found to be 9 fold higher in the case of LS174T cells compared to HEK-293.

232

233   **CEA-Affimers successfully target cubosomes to CEA expressing colorectal cancer cells**

234   Affimer tagged cubosomes labelled with the green fluorescent lipid NBD-PE (Cbs-NBD) were

235   added to CEA expressing LS174T cells and were found to be endocytosed, as suggested by the

236   green fluorescence observed around the cell nucleus, in the cytoplasmic region of the LS174T cells

237   after a period of 24 h (**Figure 3A-B**). On the contrary, fluorescent cubosomes that where not

238   Affimer tagged showed little uptake by the LS174T cells during the timeframe of the experiment.

239   It has been shown that PEGylation of nanoparticles can hinder cell-nanoparticle interactions due

240   to steric hindrance and consequently a target moiety is needed to overcome this barrier and

241   promote uptake via receptor mediated endocytosis[40-41, 53]. Our results suggest that Affimer tagged

242   cubosomes show promise in selectively delivering cargo to CEA expressing cells.

243
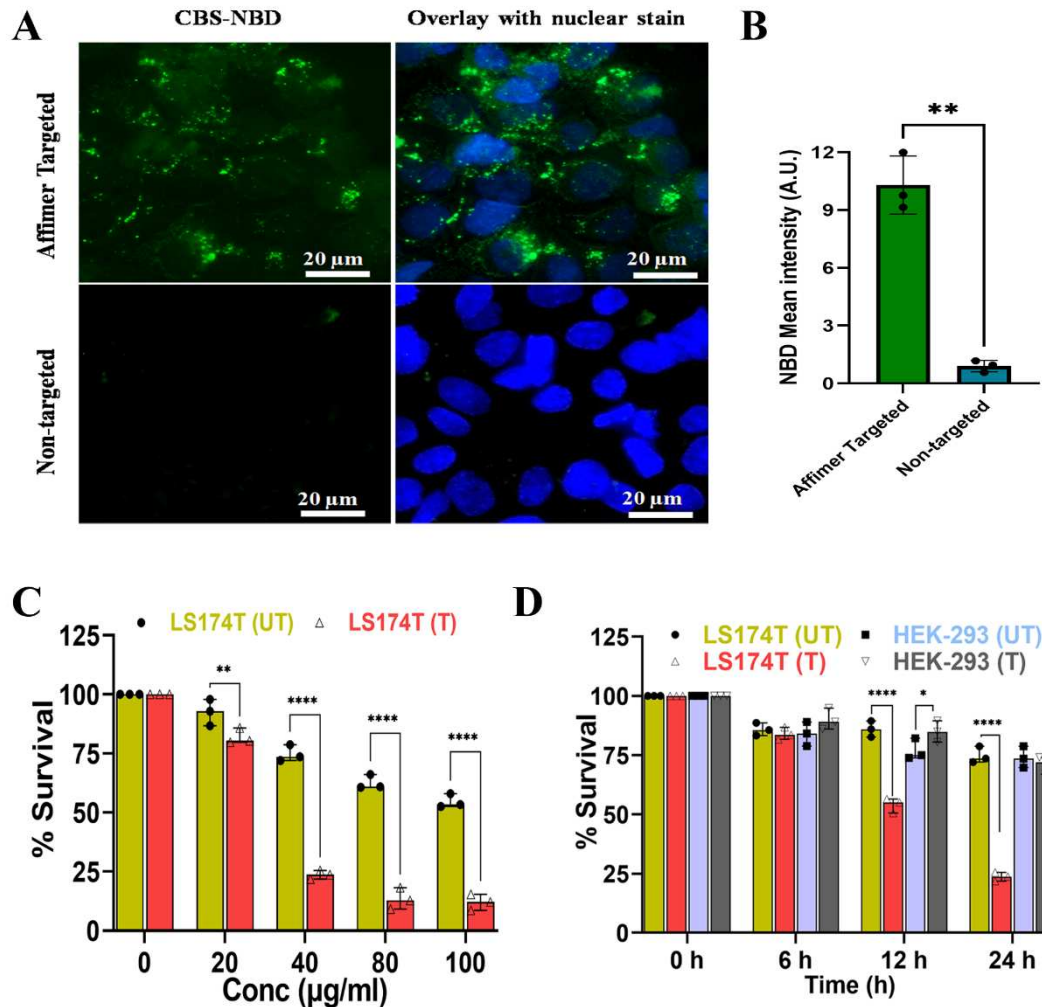
Figure 3: *In vitro* localization and targeting efficiency of Affimer labeled cubosomes; (A) Localization of fluorescently labelled cubosomes (Cbs-NBD) in LS174T with and without Affimer tagging. Cbs-NBD were observed at the cytoplasmic region of the cells post 24h treatment when tagged with Affimer whereas CBS-NBD uptake was negligible in the absence of Affimer, showing specificity of Affimer tagged cubosomes towards CEA expressing LS174T cells. (B) Quantitative analysis of Cbs-NBD (i.e. green florescence) shows a significant increase of 9.5 fold (**p<0.01 using Welch's non-parametric t-test) when Affimers are tagged to the cubosome compared to non-targeted cubosome in LS174T cells. (C) Cytotoxicity evaluation of Cbs-Cu i.e untargeted represented as 'UT' and Cbs-Cu-Af i.e Affimer targeted represented as 'T' in LS174T cells at concentration range between 0 - 100μg/ml. There was a significant decrease (****p<0.0001, **p<0.01 using two-way ANNOVA) of survivability of the cells when CuAc was delivered via Cbs-Cu-Af. This observation was noted with dose starting from 40 μg/ml. (D) Cell viability of LS174T and HEK-293 cell lines with 40 μg/ml of Cbs-Cu 'UT' and Cbs-Cu-Af 'T' at various time points up to 24h. Significant reduction (****p<0.0001 using three-way ANNOVA) of survivability in LS174T cells is evident when treated with Cbs-Cu-Af but has a negligible effect

13

260 on HEK-293 cells as they lack the CEA expression. Without Affimer 'UT' there was negligible
261 toxicity in either of the cell lines.

262
263
264 **Affimer tagged cubosomes show selective toxicity to colorectal cancer cells- *In vitro* studies**

265 Monolayer 2D cultures of LS174T and HEK-293 cells were chosen for studying the drug

266 targeting efficiency of Affimer tagged cubosomes. Bare cubosomes were studied for their

267 biocompatibility in cells which concluded no cytotoxicity in both cell lines at a concentration of

268 up to 100 μg/ml (**Figure S11**). To identify an optimum concentration of CuAc (5 wt%) loaded

269 cubosomes, LS174T cancer cells were initially screened under varying concentrations (0 - 100

270 μg/ml) of Cbs-Cu (with and without Affimer) for a period of 24 h. A concentration of 40 μg/ml

271 showed a significant decrease in cell viability, with the Affimer targeted and non-targeted

272 cubosomes showing a survival rate of 21 ± 6% and 75 ± 4% respectively (**Figure 3C**). Further

273 cytotoxicity studies were performed at 40 μg/ml in both the cell lines (with and without Affimer

274 tagging) at varying time points over a period of 24 h. The non-cancerous HEK-293 cells showed

275 no significant reduction in cell viability (80 ± 5%) when treated with both targeted and non-

276 targeted Cbs-Cu (**Figure 3D**). Contrastingly, although LS174T cells showed a high cell viability

277 when treated with non-targeted cubosomes, Affimer tagged cubosomes showed a significant drop

278 in cell viability (52± 4%) after 12 h (**Figure 3D**). This result is in agreement with our cubosome

279 localization study above, and suggests that Affimer tagged, drug loaded cubosomes are taken up

280 by cells within a 6-12 hour period, whereas non-cancerous CEA negative cells displayed minimal

281 uptake and cytotoxicity and show promise in targeted delivery to CEA expressing cells with low

282 toxicity to normal cells. This is the first demonstration of Affimer-directed specific cancer cell

283 death using drug-loaded cubosomes. Cell death of the LS174 CEA-expressing cell line treated with

284 targeted cubosomes was shown to be mediated by apoptosis (**Figure S12**). A clear difference is

285   seen in Affimer tagged and untagged cubosomes in efficiency of targeting, that proves Affimers

286   are active even after tagging on cubosomes.

287
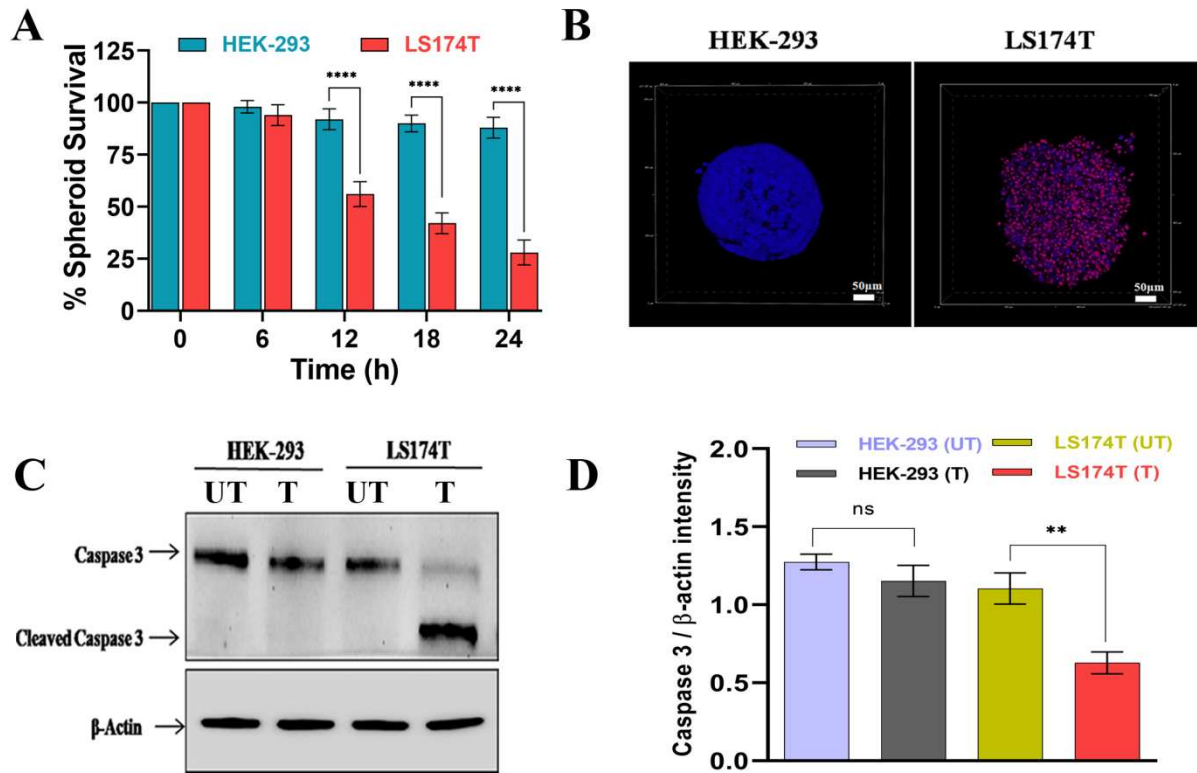
Figure 4: 3D Spheroid study of Affimer targeting; (A) Survivability study of 40 μg/ml Cbs-Cu-
Af on 3D spheroids of LS174T and HEK-293 up to 24h of treatment. The survivability was
measured using the intensity of red (propidium iodide) and blue (Hoechst 33342) fluorescence
denoting dead and live cells respectively. LS174T spheroids had a significant reduction
(****$p<0.0001$ using two-way ANNOVA) in survivability after 12h whereas negligible effects
were observed in HEK-293 spheroids even after 24h. (B) Confocal images of the spheroids after
24h treatment with 40 μg/ml Cbs-Cu-Af showing the above observation. (C) Whole cell lysate
from the spheroids after 24h treatment of Cbs-Cu with Affimer tagged delivery 'T' or without
Affimer 'UT' were analysed for apoptosis using western blot of Caspase 3 marker. (D) Intensity
plot for caspase 3 from the blot. From the band intensity measurement it was evident that in case
of LS174T spheroids there was a significant decrease (**$p<0.01$ using un-paired t-test) in full
length caspase indicating apoptosis only in the LS174T cells upon Affimer tagged delivery of Cbs-
Cu whereas no significant sign of apoptosis in case of HEK-293 spheroids.

301

302

303   3D tumor spheroids are considered to be much more relevant models, in order to evaluate drug

304   efficacy and mimic solid tumors *in vivo*, as compared to conventional monolayer 2D cultures[54-55].

305   The cytotoxicity of Cbs-Cu-Af (40 μg/ml) on spheroid models of both HEK-293 and LS174T cell

306   lines was studied and it was observed that after 24h of treatment, HEK-293 spheroids showed a

307   survivability of 88 ± 5% whereas a significant drop of 30 ± 6% was noted in the case of LS174T

308   spheroids (**Figure 4A-B**). It has been shown that 3D spheroids can be more resistant to drugs and

309   delivery vehicles compared to 2D cultures[9, 56]. Although the survival rate of LS174T spheroids is

310   slightly higher than the 2D culture data, Cbs-Cu-Af cubosomes are effective in specific targeting

311   in the spheroid models. This finding was further validated with western blot studies, using a

312   caspase 3 marker and confirmed that Cbs-Cu-Af cubosomes induced apoptosis[38] upon targeted

313   delivery in LS174T cells (**Figure 4C-D**).

314

315   **Affimer functionalized cubosomes show targeted release of payload in tumors *in vivo***

316   Having shown that Cbs-Cu-Af cubosomes could preferentially target CEA positive LS174T

317   cells to deliver the drug, their ability to target tumors in *in vivo* models was investigated. We used

318   subcutaneous (heterotopic) xenograft tumours of LS174T cells as our model, since subcutaneous

319   models provide a suitable environment for testing pharmacology and activity of novel agents.[57]

320   Fluorescent dyes have been either been encapsulated or tagged on cubosomes to study their

321   localization *in vivo*[9, 25]. Here we chose a far-red-fluorescent hydrophobic Cy5 dye to study the

322   localization of Affimer tagged cubosomes in *in vivo* models. Whole organs of mice (brain, liver,

323   kidney, spleen, heart, lung along with the tumor), were quantified for their Cy5 fluorescence by

324   *exvivo* IVIS imaging upon delivery of the Cy5 loaded Affimer tagged cubosomes (Cbs-Cy5-Af),

325   with a suitable control (Cbs-Cy5) at various time points (**Figure S13A-B**). As observed in **Figure**

326   **5A**, after a period of 72 h post administration, the fluorescence intensity indicated the accumulation

327   of Cy5 mainly in the tumor regions (indicated by an arrow) of the Affimer targeted mice group

328 (Cbs-Cy5-Af). For the control group (Cbs-Cy5 cubosomes), the concentration of dye was noted to

329 be maximum in the liver. As observed in our *in vitro* study (**Figure 3**), we hypothesize that the

330 Affimer tagged cubosomes are preferentially taken up by the tumor cells via receptor mediated

331 endocytosis, followed by an interaction with the endolysosomal compartment leading to the release

332 of the payload[58]. A significant increase in Cy5 intensity was noted in tumor tissues of the targeted

333 group as compared to non-targeted group (**Figure 5B**). A high level of accumulation of therapeutic

334 nanoparticles in the liver has been noted as a common bottleneck to their applications[59]. A few

335 studies have shown that cubosomes can improve the efficacy of drugs loaded in them, however

336 there is a scarcity of knowledge on how these nanoparticles behave *in vivo*, as well as their

337 biodistribution. The handful of studies that have reported on this have shown that biodistribution

338 depends on the route of administration, with lipid nanoparticles administered intravenously

339 preferentially accumulating in the liver, spleen and kidneys [3, 11, 16]. These results differ to our

340 findings and we attribute the preferential accumulation in the tumor to active targeting using

341 Affimer tagged cubosomes. Moreover, although it is known that smaller nanoparticles are

342 absorbed by the kidneys, heart, lung and brain in addition to the liver and spleen [60], our fluorescent

343 cubosomes showed essentially no accumulation in these organs, indicating an absence of non-

344 specific cubosome absorption in either of the mice groups (targeted and non-targeted) as seen in

345 the IVIS images (**Figure 5A-B**). To further validate these findings, tissue sections of kidney, liver

346 and tumor were examined for Cy5 uptake by confocal microscopy (**Figure 5C**). Similar to the

347 above observations, Cy5 absorption was found to be 5-7 fold higher in the tumor tissue of the

348 targeted group (Cbs-Cy5-Af) as compared to the non-targeted group administered with Cbs-Cy5

349 (**Figure 5D**). A 3-dimensional reconstruction of the tumor tissue sections of the targeted and non-

350 targeted groups are shown in **Figure S13C**. Similar to our *in vitro* targeting results, Affimer tagged

351 cubosomes could selectively deliver the payload to the tumor tissue and show promise as novel

352 nanocarriers with proven biosafety and biodistribution features.

353
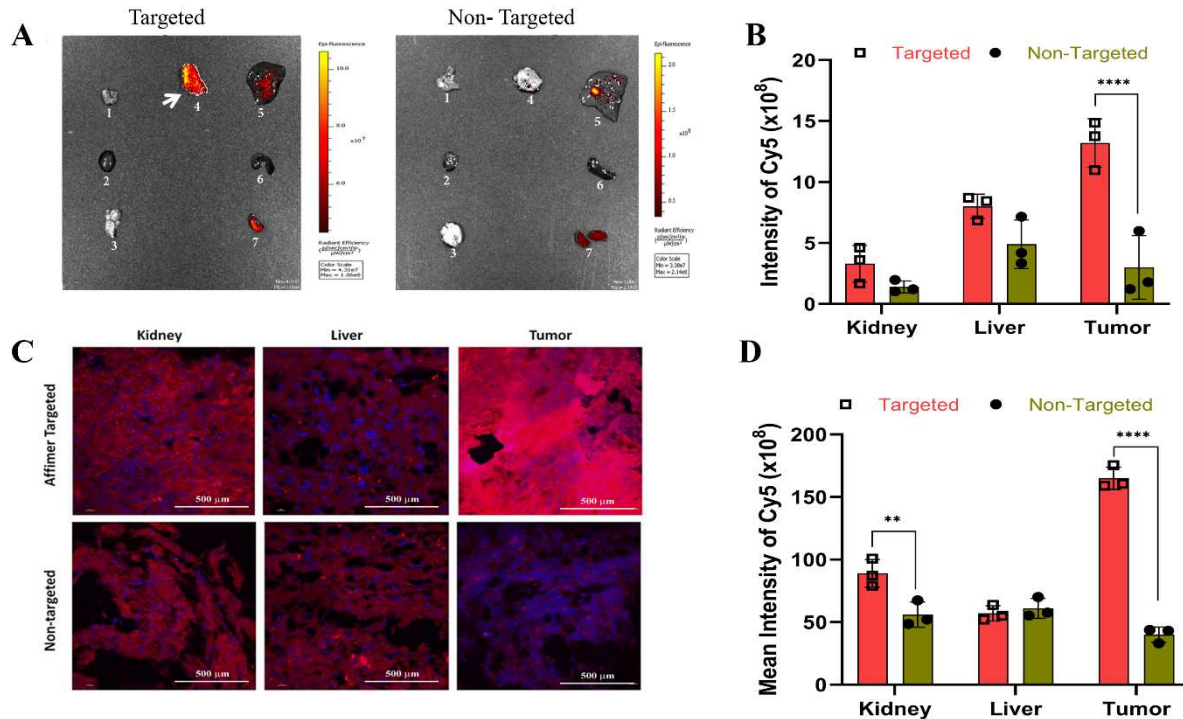
Figure 5: *In vivo* tracking of cubosomes by Cy5 fluorescence. (A) IVIS images of whole organs namely lung, heart, brain, tumor, liver, spleen and kidney as numbered from 1-7 in the image, showing uptake of Cy5 in various organs in the Affimer targeted and non-targeted groups of mice after 72h of administration. As evident, Cy5 accumulation is maximum in the tumor for the targeted group compared to the non-targeted group. Note the use of different scales in the two images that maximises the dynamic range of detection; the scale used for the targeted image is less sensitive and therefore under-represents the relative intensities when compared to the non-targeted (B) Quantitative fluorescent intensities of the IVIS image in the kidney, liver and tumor of both groups. Significant increase (****p<0.0001 using two-way ANNOVA) of Cy5 was observed in tumor of group administered with Affimer targeted delivery whereas non-targeted group showed the maximum accumulation in the liver. (C) Tissue uptake of Cy5 was studied in 5μm tissue sections of kidney, liver and tumor of both groups using confocal microscopy, (D) along with their quantitative mean fluorescence intensities. Tumor tissue uptake of Cy5 was found to be maximum (****p<0.0001 using two-way ANNOVA) in the Affimer targeted (Cbs-Cy5-Af) group whereas in the non-targeted group (Cbs-Cy5), maximum upatake was shown in the kidney and liver.

Cubosomes have promising therapeutic efficacy upon targeted delivery to the tumor xenograft

The key indicators for successful targeted delivery of a chemotherapeutic drug in mice include restricted tumor growth, increase survivability and low signs of organ toxicity[40-41]. Ultrasound imaging was used to record the tumor volumes of mice administered with saline (control), Cbs-Cu (non-targeted) and Affimer targeted (Cbs-Cu-Af) cubosomes and were recorded as a function of time (**Figure S14**). The 3-dimensional reconstruction of the tumor volume on day 16 showed significant inhibition of tumor growth in the Affimer targeted group (**Figure 6A**). The mean tumor volume was noted to be 115 ± 52.0 mm^3, 254 ± 96.0 mm^3 and 279 ± 147.0 mm^3 for the Affimer targeted, for non-targeted and control groups respectively (**Figure 6B**). The fold increase in tumor volume was calculated with reference to the treatment start V0 (day 11). The mean fold increase in tumor volume was found to be 4.4 ± 2.5, 8.2 ± 2.1 and 11.3 ± 7.3 for Affimer targeted, non-targeted and control groups respectively (**Figure 6C**). As evident from **Figure 6C**, data scatter in the case of the Affimer targeted group was found to be the least, which is in accordance with reports on *in vivo* studies of cisplatin targeted delivery using hyaluronic acid [40], or a paclitaxel formulation targeted by a RGD peptide[41], where the tumor volume was recorded and a size reduction of about 66% was observed in the targeted group. One of the routine assessments to evaluate the toxicity arising from drug administration is indicated by a change in body weight or a loss of weight in mice[40, 61]. The body weight of mice was recorded at regular intervals during the study. Results showed a gradual increase (although within 10%) in the control group with minimal effects in the other two groups thereby indicating a minimal effect on the welfare of the mice upon treatment (**Figure 6D**). As shown in **Figure 6E**, the survivability of CRC tumor xenograft bearing mice was assessed in the three groups post treatment; survival was denoted as the tumor volume

reaching the maximum permissible diameter of 17 mm. Survivability and the extent of drug toxicity could be directly correlated with the efficacy of the therapeutic[41]. A successful targeted delivery would result in enhanced welfare of the animal survival ensuring a minimal sign of toxicity[41, 61]. In our study, the survival of the control group was reduced to 40% on day 13 and 20% on day 16. The group of mice administered with Cbs-Cu-Af showed a maximum survival of 80% on day 16 as the tumor growth was restricted after targeted delivery of CuAc, whereas the group injected with non-targeted cubosomes (Cbs-Cu) showed a 40% survival. An improved survivability in the non-targeted group could be attributed to the enhanced permeability retention effect (EPR) due to the tumor vasculature[62]. Thus, these data indicate that the targeted delivery of Cu-Cb-Af has a positive impact on the mice heath and restricted the tumor growth. It would also be of value to assess in the future this effect in orthotopic models, especially of locally disseminated disease,[63] for which systemic targeted therapeutics have real potential to impact on clinical outcomes.
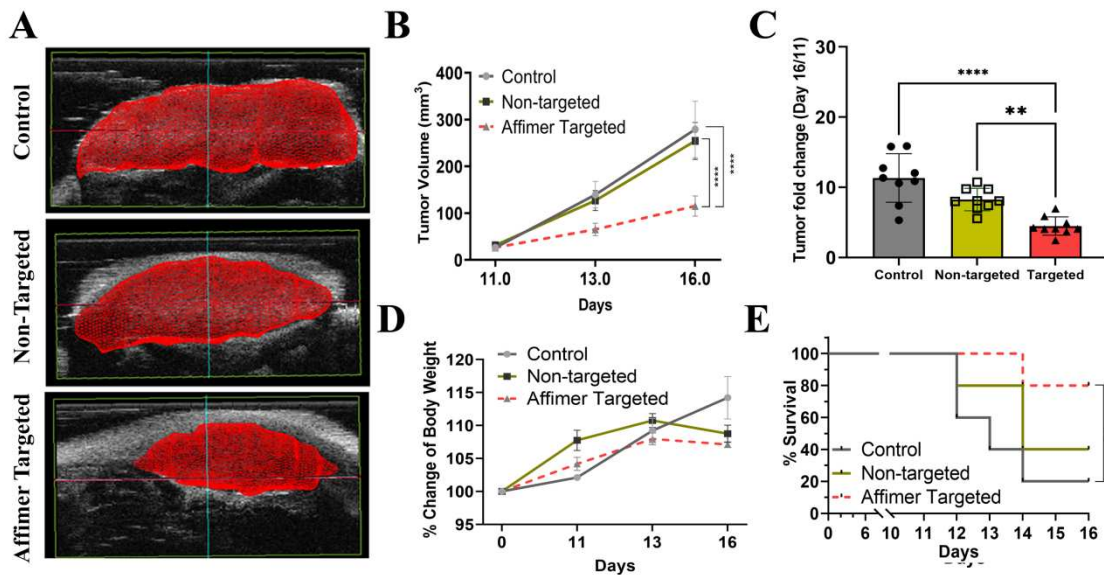
Figure 6: Efficacy of Affimer mediated drug delivery *in vivo*. (A) 3D reconstruction of ultra-sonography (USG) measured tumor volume of the three groups i.e. control (saline), non-targeted (Cbs-Cu) and Affimer targeted (Cbs-Cu-Af) administration showing tumor growth restriction in the case of the Cbs-Cu-Af. (B) Quantitative data of tumor volume as recorded in the three groups by USG on day 11, 13 and 16 where it is evident that after the 1st dose of administration on day 11, tumor growth was restricted in the targeted group. Here using unpaired t-test, statistical analysis of day 16 shows a significant difference (****$p<0.0001$) between targeted and control group as well as (****$p<0.0001$) targeted and non-targeted group. (C) Data representing the fold change in tumor volume from day 11 to day 16 in the groups which shows post targeted delivery of Cbs-Cu resulted in significant reduction (using one-way ANNOVA) of tumor growth compared to control (****$p<0.0001$) as well as non-targeted group (**$p<0.01$). (D) Change in the body weight of mice in the three groups during the study were measured and no reduction of body weight (as a sign of toxicity) was noted. (E) Survival rate of mice in the groups represented by a Kaplan Meier Curve as per the tumor volume reaching the permissible limit and hence euthanized. Using logrank test a significant increase (*$p<0.05$) of survivability was noted in targeted group compared to control group. The survivability of Affimer targeted group was 80% on day 16 whereas in control and non-targeted, they were 20% and 40% respectively.
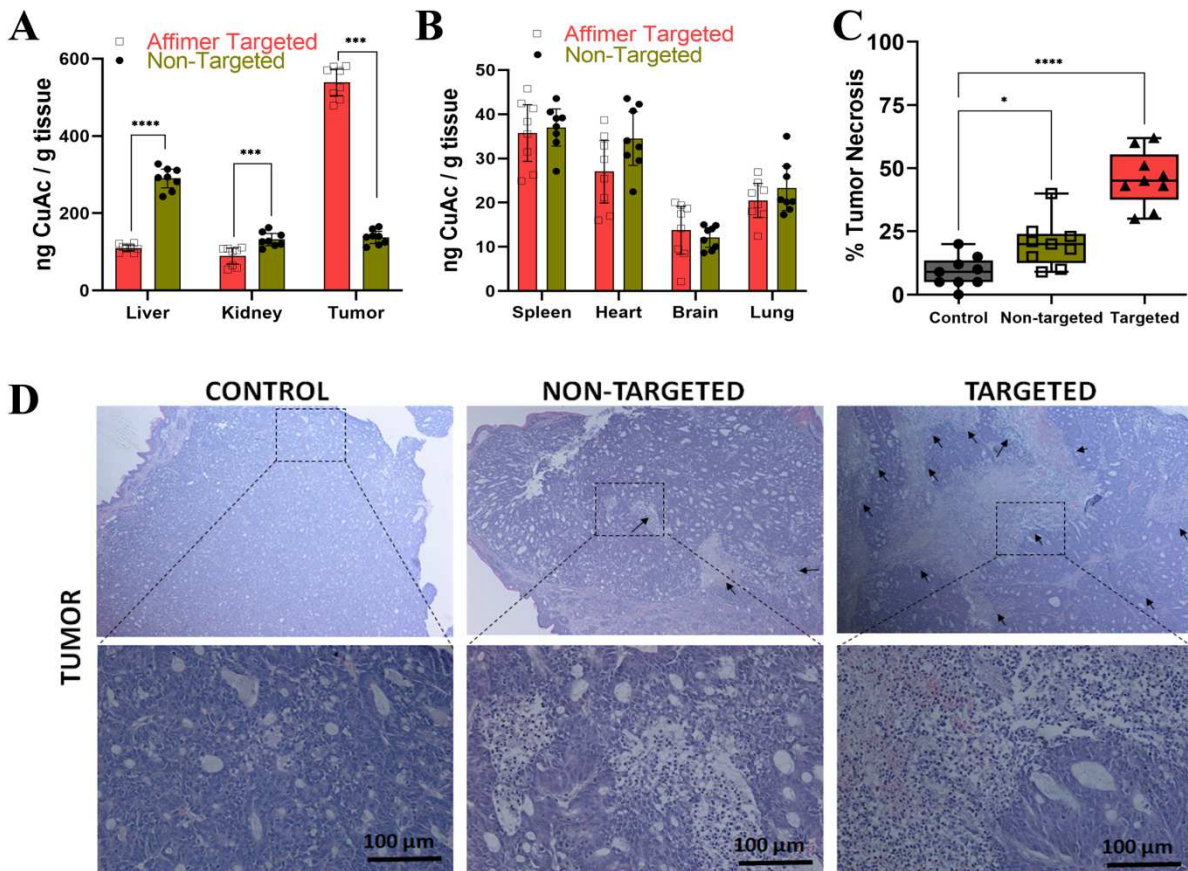
Figure 7: Biodistribution of CuAc in organs and biosafety study upon Affimer targeted delivery of CuAc encapsulated cubosomes. ICP-OES data of CuAc uptake in the (A) liver, kidney and

tumor of the non-targeted (Cbs-Cu) and Affimer targeted (Cbs-Cu-Af) groups. A significant increase (****$p<0.0001$ using 2-way ANNOVA with Bonferroni's correction) in CuAc uptake in tumor tissue of the Affimer targeted group was noted whereas accumulation was highest in the liver for non-targeted.(B) Tissue absorption of CuAc measured from ICP-OES in other organs such as spleen, heart, brain and lung was negligible and well below the limits of any safety concern.(C) Quantitative tumor tissue necrosis data as studied by Haematoxylin and Eosin (H&E) staining along with (D) the microscopy images of tumor tissue sections of the three groups. A significant increase (****$p<0.0001$) in tissue cell death was noted for the Affimer targeted group compared to the control which indicates CuAc having maximum effect on tumor upon targeted delivery.

Drug safety is assessed based on its effect on vital organs [40-41, 64] and one such method to analyze the toxicity is an in-depth tissue study. Inductively coupled plasma optical emission spectrometry (ICP-OES) has been used in the past to determine the accumulation of metal based drug such as platinum in various organ[60, 65]. Here we used ICP-OES to estimate Cu uptake as a reference to CuAc distribution in homogenised organ samples, including the liver, kidney, spleen, heart, brain, lung along with tumor. In the targeted delivery of Cbs-Cu-Af mice group, the maximum uptake of CuAc was noted in the tumor tissue, whereas in the non-targeted group, major uptake was found to be in liver followed by moderate amounts in the tumor and kidney. A comparison between targeted and non-targeted groups suggests an approximately 4.5 fold increase in CuAc uptake in the tumor tissue of the targeted group, which is similar to our findings on the Cy5 distribution as shown in **Figure 5**. The uptake of CuAc was approximately 5 fold higher in the tumor compared to the kidneys and liver for the targeted groups of mice (**Figure 7A**). Thus, these data indicate specificity of Cu-Cb-Af cubosomes towards tumor cells with up to 550 ng of CuAc per gram of tissue accumulation, compared to non-targeted Cu-Cb cubosomes which had about 120 ng of CuAc per gram of tissue. Other tissues of spleen, heart, brain and lung had negligible CuAc accumulation (**Figure 7B**).

457 Haematoxylin and Eosin staining of tissue sections is common practice to study toxicity associated

458 with drugs[40, 66]. Tumor cell death was studied in the tissue sections for all three groups (**Figure 7C-**

459 **D**).The percentage of dead cells in the tumor tissue were measured in all groups and showed that

460 targeted delivery resulted in a significant increase in tumor cell death (**Figure 7C**) compared to

461 non-targeted delivery which was almost 2.5 to 3 times higher. Yet again, the significant cell death

462 in the non-target tumor group could be due to the EPR effect. Similar to the study for doxorubicin

463 delivery in colon cancer by Wei *et al.*, [66], we further confirmed the safety of this drug

464 administration by examining tissue sections of the heart, liver and kidney of the three groups by

465 histology. As seen in **Figure S15**, no significant signs of cell death (i.e. organ toxicity) was

466 observed in both targeted and non-targeted delivery groups which could be attributed to the

467 absence of CEA expression in those cells. Further, tissue sections of lung, brain, and spleen

468 (**Figure S16**) of targeted and non-targeted groups were also examined and no tissue cell death was

469 noted. Hence the data and observations could be correlated to the biosafety of the drug loaded

470 nanocarrier.

471

472 **CONCLUSION**

473 We have developed monoolein based cubosomes, with an internal nanostructure based on space

474 group Im3m, that have been functionalized for the first time with an Affimer protein via copper-

475 free click chemistry to actively target carcinoembryonic antigen expressing colorectal cancer cells.

476 The cubosomes could selectively target the cancer cells both *in vitro* (2D monolayer cultures and

477 3D spheroid models) and *in vivo*. Targeted cubosomes, loaded with the model anticancer drug

478 copper acetylacetonate, showed high efficacy in the tumor tissue of mouse xenografts and resulted

479 in significantly restricting tumor growth, a high survival rate compared to the control groups, no

480 signs of toxicity and low non-specific tissue absorption in other vital organs. Due to the limited

481 studies on actively targeted, drug loaded cubosomes, as well as their performance and efficacy *in*

482 *vivo*, we hope these results will add to the growing body of knowledge of cubosomes as promising

483 delivery vehicles for cancer therapy and shed light into their biodistribution and efficacy *in vivo*

484 that may aid to clinical translation of these promising lipid nanoparticles.

485

486 **MATERIALS AND METHODS**

487 **Clickable cubosome preparation and payload encapsulation**

488 Cithrol™ GMO (MO) was a kind gift from Croda (Croda Personal Care, Goole, UK), and is a

489 commercial version of monoolein, containing a minimum of 92% monoester and a maximum 8%

490 diester. DSPE-PEG-2000 azide (DPA) was purchased from Avanti Polar Lipids (AL, USA) and

491 Pluronic® F-127 from Sigma-Aldrich (Gillingham, U.K.). Bare cubosomes were prepared using

492 various ratios of MO (90-95% w/w) : DPA (5-10% w/w) co-dissolved in chloroform (Merck, New

493 Jersey, USA) and dried under nitrogen gas. To ensure all solvent had evaporated the dry lipid films

494 were left in a desiccator overnight at room temperature. The lipid films were hydrated with

495 phosphate-buffered saline (PBS; Sigma-Aldrich Gillingham, U.K) containing Pluronic® F-127.

496 The concentration of F127 was varied between 2 to 7 wt% of the MO. Nanoparticle dispersions

497 were prepared by tip sonicating the sample in 1mL of buffer using a Q125 sonicator

498 (Qsonica,USA) for 30 minutes in pulse mode (1s pulse on, 1s off) at 80% amplitude in an ice bath.

499 The resultant cubosomes were then passed through a mini extruder (Avanti Polar Lipids, USA)

500 using a 100 nm pore size polycarbonate membrane (Whatman, USA). For drug loaded cubosomes,

501 copper acetylacetonate (CuAc; Merck, USA) was dissolved in chloroform and added in various

502 amounts (1- 5% w/w) to the co-dissolved lipid mixtures. The same steps described above for bare

503 cubosomes were then followed. The drug loaded cubosomes were placed in Slide-A-Lyzer

504 cassettes (2K MWCO, Thermo Scientific, UK) in PBS at 25ºC to remove any free CuAc. The

505 external PBS was changed at regular interval while performing the dialysis.

506 For studying cubosome localization by fluorescence *in vitro*, 0.5% w/w of 1,2-dioleoyl-sn-glycero-

507 3-phosphoethanolamine-N-(7-nitro-2-1,3-benzoxadiazol-4-yl) (ammonium salt)(18:1-NBD PE;

508 Avanti Polar Lipids, USA) was co-dissolved with the lipid mixtures in chloroform before the

509 drying step. For the *in vivo* fluorescent studies, 2% w/w of Cy5 dye (MedChemExpress, USA) was

510 co-dissolved with the lipid mixtures in chloroform. As with the CuAc loaded cubosomes, Cy5

511 labelled cubosomes were loaded in dialysis cassettes to remove any free dye.

512 Inductively coupled plasma optical emission spectrometry(iCAP™ 7600 ICP-OES Analyzer,

513 Thermo Scientific, UK) equipped with a 240-position Cetac auto-sampler was used to estimate the

514 amount of coppen as an indicator of CuAc encapsulated in the cubosomes using a known

515 concentration of copper solution as a standard curve. The encapsulation efficiency (%) was

516 calculated using equation (1):

517 $$EE\ (\%) = (M1/M2)\ \text{x}\ 100 \tag{1}$$

518 where M1 represents the weight of drug encapsulated in mg (obtained from ICP-OES) and M2

519 represents total drug added (mg) to the cubosomes.

520 **Affimer cloning and production**

521 Anti CEA specific Affimer clones were identified using a 'phage display library' method as

522 recently published by Shamsuddin *et al*. [35]. Out of the three CEA binding Affimers identified,

523 clone II and III were chosen for this study having 9 and 10 distinct amino acid residues at the

524   variable region respectively in clone II and clone III. Based on a 50 ml of working volume, the

525   yield of the Affimers were noted to be 8.3 mg and 6.27 mg for clone II and III respectively [35-36]

526   with corresponding molecular weights noted to be 12.5 and 12.6 kDa (**Figure S4A**). The associated

527   DNA from the positive clones were sequenced. The coding region of the selected Affimers were

528   amplified by PCR during which a cysteine codon at the C-terminal was inserted for the ease of

529   functionalization. The Affimer coding sequence was inserted into the pET11a vector using two

530   restriction enzymes NheI-HF and NotI-HF and then Affimer production was done in BL21 (DE3)

531   E.coli cells as previously reported[32]. The E.coli cells were grown in Luria-Bertani broth medium

532   containing 100 µg/ml of carbinicillin until the growth absorbance value was 0.8 at 600 nm. Then

533   cells were induced with 0.1 mM IPTG and incubated at 25°C for 6 h. The cells were harvested by

534   centrifugation, lysed and the His_8 tagged Affimers were purified on Ni2+-NTA affinity

535   chromatography (Merck, New Jersey, USA). The binding efficiency of these Affimers to the CEA

536   receptor was thoroughly studied and confirmed using surface plasmon resonance as reported by

537   Shamsuddin et al.[35] The surface plasmon resosnace showed that the Affimers demonstrated a high

538   binding affinity towards CEA (K_D value for clone II:15.3 ± 0.37 nM; K_D value for clone III:

539   34.4 ± 16 nM) (**Figure S4B**).

540

541   **Functionalization of cubosomes with Affimers**

542   Affimers were attached to the cubosomes using DBCO-maleimide (Kerafast, Inc. Boston, USA)

543   click coupling chemistry. Briefly, 2 ml of (0.5 mg/ml) Affimer clone II and clone III were reduced

544   using 150 µl (5.7 mg/ml) TCEP-HCl (Merck, New Jersey, USA) for 90 min to remove any dithiol

545   linked dimers. The reduced Affimers were incubated with 4 mM DBCO-maleimide for 2 h to

546   attach DBCO and then 100 mg/ml azide containing cubosomes were added to allow click coupling

547 to occur and incubated for overnight at room temperature. The final product was dialysed for 24h

548 in 1x PBS using Slide-A-Lyzer Dialysis Cassettes, 5K MWCO (Thermo Scientific, Waltham,

549 USA) to remove unreacted Affimers. FTIR spectroscopy (Platinum ATR , Model – Alpha, Bruker,

550 UK) was used to confirm the covalent conjugation between the azide group of cubosomes and the

551 DBCO group attached to the Affimers.

Small angle X-ray scattering

553   The internal nanostructure of the cubosomes was probed with small angle X-ray scattering

554 (SAXS). The measurement were done at 25ºC and 37 ºC (5 minute equilibration at the desired

555 temperature with and accuracy of ±0.1°C) for all three samples: bare cubosomes, drug loaded

556 cubosome (Cbs-Cu) and Affimer tagged drug loaded cubosomes (Cbs-Cu-Af). Synchrotron SAXS

557 measurements were carried out on beamline I22 at Diamond Light source. The synchrotron beam

558 was tuned to a wavelength of 0.69 Å with a sample to detector distance of 3.7 m and the 2-D SAXS

559 patterns were recorded on a Pilatus 2M detector. SAXS experiments were also conducted on a lab-

560 based Xeuss 3.0 (Xenocs, , France) beamline equipped with a liquid gallium MetalJet X-ray source

561 (Excillum, Sweden) which has an energy of 9.2 keV, corresponding to a wavelength of 1.34 Å. 2-

562 D SAXS patterns were recorded on a Eiger2 R 1M detector (Dectris, Switzerland) and the sample

563 to detector distance was set to 0.8 m giving a q range of 0.01-0.4 Å-1. Silver behenate (a = 58.38

564 Å) was used to calibrate the SAXS data. SAXS images were analysed using the IDL-based AXcess

565 software package or the DAWN software[67-68].

Dynamic Light Scattering (DLS)

567 The hydrodynamic diameter i.e. the particle size of all cubosome samples were measured at 25 °C

568 using a dynamic light scattering (DLS) instrument Zetasizer Nano ZS90 (Malvern Panalytical,

569 Malvern, UK) at a fixed backscattering angle of 173°. The refractive index of the cubosomes was

570 set to 1.46 (pure MO) with an absorbance of 0.10. The refractive index of the dispersant (PBS)

571 was set to 1.332 with viscosity 0.9053cP.

572 The size of Cbs, Cbs-Cu and Cbs-Cu-Af samples were measured by adding $100\mu l$ of cubosomes

573 into $900\,\mu l$ of PBS in a 3ml cuvette. The instrument equilibration time was set for 120 sec at 25ºC

574 and samples ran for 10 cycles with 10 measurement in each cycle. For zeta potential

575 measurements,$100\,\mu l$ of Cbs-Cu-Af was added to $900\,\mu l$ of water (with a resistivity of $18.2\,M\Omega.cm$

576 at 25 °C) in a disposable zeta cuvette and the sample was equilibrated for 120 sec at 25ºC. The

577 instrument was set to run 20 cycles with 10 measurements in each cycle.

578 **Transmission Electron Microscopy (TEM)**

579 Morphological analysis of the Cbs-Cu-Af cubosome was done using a high resolution transmission

580 electron microscope (FEI Tecnai TF20) fitted with field emission gun TEM/STEM along with

581 HAADF detector. For this study, a 200 mesh Carbon film coated on Nickel grid (EM Resolutions,

582 UK) was used. 10 μl of Cbs-Cu-Af (10mg/ml) in PBS was added on the grid and any excess

583 droplets were soaked up using an absorbent filter paper. The grid was left in a desiccator to dry for

584 24h. The sample was imaged at 13,000x magnification at an accelerating voltage of 300kV. The

585 image was captured using a Gatan Orius SC600A CCD camera. Further images were analyzed

586 using Fiji ImageJ software (NIH, USA). The same sample was analysed by energy dispersive X-

587 ray equipped in the FEI Tecnai TF20 (Oxford Instruments INCA 350 EDX system/80mm X-Max

588 SDD detector) to study the presence of CuAc in the cubosome (copper as a marker). The advantage

589 of using a nickel grid over a standard copper grid in this study was to eliminate any background

590 noise of copper during this EDX study.

Cryogenic Transmission Electron Microscopy (cryo-TEM)

Cubosomes at a concentration of 79 mg/ml where used for the morphological characterization using cryo-TEM. 3μL of sample was deposited to freshly glow discharged Cu QUANTIFOIL grids (R2/R2, 300 mesh) with a holding time of 30 s. The carbon coated grids were glow discharged at 10 mA for 20 s and blotted for 6 s (blotting force of 7 at 25 °C under 100% relatively humidity). The grids were subsequently plunged into liquid ethane using a Vitrobot™ mark IV (Thermo/FEI). A Titan KRIOS microscope (Thermo Fisher Scientific, US) with an accelerating voltage of 300 KV and a defocus value of -4 μm was used to image the cubosomes at a magnification of 47000 which has a pixel size of 1.76 Å. Image processing and analysis was done using Fiji . Indexing of the cubosome was determined by obtaining the d-spacing of each reflection in the FTT using TrackMate.[69]

Cell culture

CRC cell line LS174T and non-cancerous HEK-293 cells were originally obtained from ATCC and were subjected to mycoplasma testing and STR typing (Source Bioscience, UK) before use. Cells were grown in DMEM (Thermo Scientific, Waltham, USA) growth medium supplemented with 10% (v/v) fetal calf serum (FCS; Thermo Scientific, Waltham, USA) and penicillin/streptomycin (Thermo Scientific, Waltham, MA, USA) at 100 units/ml. All cells were cultured in a humidified incubator with 5% CO_2 at 37 °C. Cells were maintained and experiments were conducted at cell densities that allowed exponential growth or otherwise mentioned.

Immunofluorescence assay for detecting of CEA expression

611   LS174T and HEK-293 cells were grown in complete growth medium for 48h then washed in PBS

612   and fixed with 4% (w/v) paraformaldehyde (Merck, New Jersey, USA) in PBS at room

613   temperature for 10 min. The fixed cells were further washed with PBS and permeablized with

614   0.2% (v/v) Triton X-100 (Merck, New Jersey, USA) in PBS on ice bath for 10 min. Cells were

615   then washed with PBS several times and blocked with 5% (v/v) FCS in PBS for 1 h in an ice bath.

616   Subsequently the cells were incubated with mouse anti-human IgG CEA monoclonal antibody (cat

617   no. MA5-14675, Thermo Scientific, USA) at 1μg/ml overnight at 4ºC. The following day, several

618   washes were performed with wash buffer, comprising of 0.5% (v/v) FCS and 0.05% (v/v) Tween-

619   20 in PBS. Cells were then incubated with, Alexa Fluor 488 labelled secondary antibody (cat no.

620   A-11001, Thermo Scientific, USA) at 1μg/ml for 1 h at room temperature in the dark. Cells were

621   then washed with wash buffer several times, and mounted with Fluoromount-G™ mouting media

622   with DAPI (Thermo Scientific, USA) before analyzing them under a confocal microscope (Nikon

623   A1R LSM),with a 405nm laser for DAPI with excitation and emission wavelengths of 407nm and

624   450nm. For CEA expressing detection, a 488nm laser was used with excitation and emission

625   wavelenghts of 488nm and 525nm respectively. Images were captured using a 100x objective

626   mwith a numerical aperture of 1.4. The images were analyzed using the NIS-element viewer

627   software (version 5.20.01).

Western blot analysis for CEA protein expression and apoptotic markers

629   Western blots were performed as detailed in our previous work.[38] Briefly, gel electrophoresis was

630   performed for 90 min at 120V on a 4 - 12% precast polyacrylamide gel (Bio Rad, California,

631   USA). The proteins were then transferred to a PVDF membrane and blocked with 5% (w/v) non-

632   fat skimmed milk in TBST (Tris buffered saline with 0.1% Tween-20) for 1h. The membrane post

633   blocking was labeled with respective primary and secondary antibodies and further imaged under

634   a chemi-doc instrument (Biorad, USA) after incubating with Pierce™ ECL reagent.

Confocal microscopy

636   Confocal microscopy was use to localize cubosomes *in vitro*. LS174T cells were seeded in glass

637   coated chambered slides (Thermo Scientific, USA) overnight for 18h. Next, cells were treated

638   with 20μg/ml of NBD-PE cubosomes with and without Affimer tagging for 24h. Then cells were

639   gently washed with PBS and incubated with 5μg/ml Hoechst 33342 for 15mins before imaging

640   the cells under the confocal microscope with 100x objective lens and numerical aperture of 1.4.

641   For nuclear staining (Hoechst 33342) a 405nm laser was used at excitation and emission

642   wavelength of 407nm and 450nm. For cubosome detection a laser of 488nm was used with

643   excitation and emission of 488nm and 525nm respectively. Images were captured using Galvano

644   scanning mode and analysed using the NIS-element software (version 5.20.01).

***In vitro* targeting studied in monolayer culture and 3D spheroids**

646   LS174T and HEK-293 cells were seeded in 24 well culture plates in complete DMEM growth

647   media at densities of 2.5 x 10⁴ cells/well and incubated overnight for 18 h. Cells were then treated

648   with concentrations ranging for 0 to 100μg/ml of Cbs-Cu or Cbs-Cu-Af for up to 24 h. Post

649   treatment, MTT assays were performed as detailed in our previous work.[38]().

650   For the spheroid culture, low adherent round bottom 96 well plates were used. LS174T and HEK-

651   293 cells (1000/well) were added with 200 μl of DMEM with 10% (v/v) FCS along with 2.5%

652   matrigel matrix (Corning, New York, USA). The 96 well plates were then centrifuged for 10 min

653   at 360x g and then incubated for 48h for the formation of spheroids. After 48h, the spheroids were

654   treated with Cbs-Cu-Af for varying time points ranging from 0h - 24h. Upon completing the

655   treatment period, spheroids were quantified for survivability by incubating with Hoechst 33342

656   (5μg/ml) for 30mins and propidium iodide (1.5 μg/ml) for 10mins. Red fluorescent propidium

657   iodide signified the amount of dead cells. Western blots were used to study the fate of cell death

658   using the apoptosis marker caspase 3.

659   ***In vivo* mice experiments**

660   Female BALB/c nude mice, aged 6 weeks, each weighing approximately 20 g were used for *in*

661   *vivo* targeting studies. Mice were sourced from an in-house maintained colony. All experiments

662   were performed following local ethical approval and in accordance with the UK Animals

663   (Scientific Procedures) Act 1986. Mice were housed in individually ventilated cages with a 12 h

664   day/night cycle with provisions for *ad libitum* food and water. At the end of each experiment, mice

665   were euthanized following standard procedures.

666   CRC Xenografts were developed by injecting exponentially growing cells of LS174T (5x105

667   cells), suspended in 100 μl of PBS, subcutaneously in the right flank of the mice. After 10 days

668   tumors were observed, and mice were then randomly divided into separate experiment groups as

669   indicated in each of the experiments.

670   ***In vivo* localization of cubosomes**

671   The localization of Affimer tagged cubosomes was studied by fluorescence using Cy5

672   encapsulated cubosomes (Cbs-Cy5). 30 mice with CRC xenograft, were divided into two equal

673   group sizes with 15 animals in each. One of the group received Cbs-Cy5 (non-targeted) and the

674 second group Cbs-Cy5-Af (Affimer targeted). The administration was done through the tail vein

675 of the mice with 100μl of sample, equating to 50 mg/kg of cubosome to mouse body weight.

676 Localization of the Cy5-Cb in the mice was studied using the Cy5 fluorescence filters in the IVIS

677 Spectrum (PerkinElmer, Inc., Massachusetts, USA) for a duration of up to 72h post-injection. At

678 each time point, 3 mice were euthanized and the brain, liver, kidney, spleen, heart, lungs along

679 with the tumor were scanned under the IVIS to quantify the Cy5 fluorescence. The tissues were

680 then frozen in OCT. Sections of 5 μm thickness were made using a cryostat (Leica CM3050S) and

681 were examined under a confocal microscope (Nikon A1R LSM).

682 **Efficacy of targeted drug delivery of Affimer functionalized cubosomes**

683 30 mice bearing CRC xenograft were randomly divided in three groups with 10 mice in each.

684 These groups received the following: saline (control group), non-targeted cubosome with CuAc

685 (Cbs-Cu) and Affimer targeted, drug loaded cubosomes (Cu-Cb-Af). Two doses of 100 μl of

686 intravenous injection containing 25mg/kg of body weight of cubosome (Cbs-Cu and Cbs-Cu-Af)

687 were administered at day 11 and day 13 (post tumor inoculation) in the respective group except

688 for the control group which received 100 µl saline. Tumor volumes were measured using high

689 frequency ultrasound (Vevo 770 FUJIFILM Visual Sonics Inc., Toronto, Canada) equipped with

690 a 40 MHz transducer, at regular intervals after the first dose between day 11 – 16. [70] As per ethical

691 guidelines, mice had to be euthanized as the tumor volume reached the permissible limit of 17 mm

692 of diameter. The experiment was terminated on day 16 and all mice were euthanized as most of

693 the control group reached the permissible tumor volume. Post euthanization, tumor and other vital

694 organs were collected to study by haematoxylin and Eosin staining (i.e. tissue histology). Organs

695 from mice receiving both Cbs-Cu (non-targeted) and Cbs-Cu-Af (targeted group) were

696 homogenized in de-ionized water (with a resistivity of 18.2 MΩ.cm at 25 °C) and the homogenate

697 was diluted 10 fold. Samples were then subjected to analysis using ICP-OES (iCAP™ 7600, ICP-

698 OES Analyzer, Thermo Scientific, UK) to estimate the drug uptake i.e CuAc content using Cu as

699 the reference material. The reference standard for Cu used was provided from the manufacturer

700 (Thermo Scientific, UK).

701

ASSOCIATED CONTENT

703 **Supporting Information**. Composition and size distribution of cubosomes, encapsulation

704 efficiency of CuAc and stability; Characterization of cubosomes using EDAX, FTIR and DLS;

705 Characterization of Affimers; Carcinoembryonic antigen expression on cells; Cytotoxicity of

706 CuAc on cells and mode of action; Biocompatibility and selective targeting of cubosome on

707 LS174T cells; *in vivo* cubosome distribution, efficacy on tumor and biosafety.

708

709 **AUTHOR INFORMATION**

710 **Corresponding Authors**

711 Arindam Pramanik - School of Biomedical Sciences and School of Medicine, University of Leeds,

712 Leeds, United Kingdom

713 Thomas A. Hughes - School of Medicine, University of Leeds, Leeds, United Kingdom

714 Arwen I.I. Tyler - School of Food Science and Nutrition, University of Leeds, Leeds, United

715 Kingdom

716 Paul A. Millner - School of Biomedical Sciences, University of Leeds, Leeds, United Kingdom

717 Emails: A.Pramanik@leeds.ac.uk; T.Hughes@leeds.ac.uk; A.I.I.Tyler@leeds.ac.uk;

718 P.A.Millner@leeds.ac.uk
719

Author Contributions

721 A.P., A.I.I.T. and P.A.M. conceived and designed the experiments. Z.X. performed the SAXS and

722 cryo-TEM experiments and analysed the SAXS data. A.I.I.T. analyzed the cryo-TEM data. A.P.

723 performed all the other experiments and analyzed the data. P.L.C. contributed to the design of the

724 *in vivo* experiments. T.M. and N.I. assisted A.P. with the *in vivo* experiments. A.P., Y.S.K., N.I.,

725 P.L.C., D.J., T.A.H., A.I.I.T. and P.A.M. contributed to study design. All authors interpreted the

726 results. A.P., T.A.H and A.I.I.T. co-wrote the manuscript. All authors discussed the results and

727 commented on the manuscript.

728

734

Notes

736 The authors declare no competing financial interest.

737

749

750 **REFERENCES**

751 (1) Mitchell, M. J.; Billingsley, M. M.; Haley, R. M.; Wechsler, M. E.; Peppas, N. A.; Langer, R.
752 Engineering precision nanoparticles for drug delivery. *Nature Reviews Drug Discovery* **2021,** *20*
753 (2), 101-124, DOI: 10.1038/s41573-020-0090-8.
754 (2) Barriga, H. M. G.; Holme, M. N.; Stevens, M. M. Cubosomes: The Next Generation of Smart
755 Lipid Nanoparticles? *Angewandte Chemie International Edition* **2019,** *58* (10), 2958-2978, DOI:
756 10.1002/anie.201804067.
757 (3) Zhai, J.; Fong, C.; Tran, N.; Drummond, C. J. Non-Lamellar Lyotropic Liquid Crystalline
758 Lipid Nanoparticles for the Next Generation of Nanomedicine. *ACS Nano* **2019,** *13* (6), 6178-
759 6206, DOI: 10.1021/acsnano.8b07961.
760 (4) Nguyen, T.-H.; Hanley, T.; Porter, C. J. H.; Larson, I.; Boyd, B. J. Phytantriol and glyceryl
761 monooleate cubic liquid crystalline phases as sustained-release oral drug delivery systems for
762 poorly water-soluble drugs II. In-vivo evaluation. *Journal of Pharmacy and Pharmacology* **2010,**
763 *62* (7), 856-865, DOI: https://doi.org/10.1211/jpp.62.07.0006.
764 (5) Nguyen, T.-H.; Hanley, T.; Porter, C. J. H.; Boyd, B. J. Nanostructured liquid crystalline
765 particles provide long duration sustained-release effect for a poorly water soluble drug after oral
766 administration. *Journal of controlled release : official journal of the Controlled Release Society*
767 **2011,** *153* (2), 180-186, DOI: 10.1016/j.jconrel.2011.03.033.
768 (6) Clogston, J.; Caffrey, M. Controlling release from the lipidic cubic phase. Amino acids,
769 peptides, proteins and nucleic acids. *Journal of Controlled Release* **2005,** *107* (1), 97-111, DOI:
770 https://doi.org/10.1016/j.jconrel.2005.05.015.

771 (7) Gontsarik, M.; Mohammadtaheri, M.; Yaghmur, A.; Salentinig, S. pH-Triggered
772 nanostructural transformations in antimicrobial peptide/oleic acid self-assemblies. *Biomaterials*
773 *Science* **2018,** *6* (4), 803-812, DOI: 10.1039/c7bm00929a.
774 (8) Negrini, R.; Fong, W.-K.; Boyd, B. J.; Mezzenga, R. pH-responsive lyotropic liquid crystals
775 and their potential therapeutic role in cancer treatment. *Chemical Communications* **2015,** *51* (30),
776 6671-6674, DOI: 10.1039/c4cc10274f.
777 (9) Zhai, J.; Tan, F. H.; Luwor, R. B.; Srinivasa Reddy, T.; Ahmed, N.; Drummond, C. J.; Tran,
778 N. In Vitro and In Vivo Toxicity and Biodistribution of Paclitaxel-Loaded Cubosomes as a Drug
779 Delivery Nanocarrier: A Case Study Using an A431 Skin Cancer Xenograft Model. *ACS Applied*
780 *Bio Materials* **2020,** *3* (7), 4198-4207, DOI: 10.1021/acsabm.0c00269.
781 (10) Jabłonowska, E.; Matyszewska, D.; Nazaruk, E.; Godlewska, M.; Gaweł, D.; Bilewicz, R.
782 Lipid membranes exposed to dispersions of phytantriol and monoolein cubosomes: Langmuir
783 monolayer and HeLa cell membrane studies. *Biochimica et Biophysica Acta (BBA) - General*
784 *Subjects* **2021,** *1865* (1), 129738, DOI: https://doi.org/10.1016/j.bbagen.2020.129738.
785 (11) Tran, N.; Bye, N.; Moffat, B. A.; Wright, D. K.; Cuddihy, A.; Hinton, T. M.; Hawley, A.
786 M.; Reynolds, N. P.; Waddington, L. J.; Mulet, X.; Turnley, A. M.; Morganti-Kossmann, M. C.;
787 Muir, B. W. Dual-modality NIRF-MRI cubosomes and hexosomes: High throughput formulation
788 and in vivo biodistribution. *Materials Science and Engineering: C* **2017,** *71*, 584-593, DOI:
789 https://doi.org/10.1016/j.msec.2016.10.028.
790 (12) Zabara, A.; Negrini, R.; Onaca-Fischer, O.; Mezzenga, R. Perforated Bicontinuous Cubic
791 Phases with pH-Responsive Topological Channel Interconnectivity. *Small* **2013,** *9* (21), 3602-
792 3609, DOI: https://doi.org/10.1002/smll.201300348.
793 (13) Cortesi, R.; Campioni, M.; Ravani, L.; Drechsler, M.; Pinotti, M.; Esposito, E. Cationic lipid
794 nanosystems as carriers for nucleic acids. *New Biotechnology* **2014,** *31* (1), 44-54, DOI:
795 https://doi.org/10.1016/j.nbt.2013.10.001.
796 (14) Kim, H.; Leal, C. Cuboplexes: Topologically Active siRNA Delivery. *ACS Nano* **2015,** *9*
797 (10), 10214-10226, DOI: 10.1021/acsnano.5b03902.
798 (15) Janeta, M.; Bury, W.; Szafert, S. Porous Silsesquioxane–Imine Frameworks as Highly
799 Efficient Adsorbents for Cooperative Iodine Capture. *ACS Applied Materials & Interfaces* **2018,**
800 *10* (23), 19964-19973, DOI: 10.1021/acsami.8b03023.
801 (16) Jain, V.; Swarnakar, N. K.; Mishra, P. R.; Verma, A.; Kaul, A.; Mishra, A. K.; Jain, N. K.
802 Paclitaxel loaded PEGylated gleceryl monooleate based nanoparticulate carriers in
803 chemotherapy. *Biomaterials* **2012,** *33* (29), 7206-20, DOI: S0142-9612(12)00706-5 [pii]

804 10.1016/j.biomaterials.2012.06.056 [doi].
805 (17) Saber, M. M.; Al-mahallawi, A. M.; Nassar, N. N.; Stork, B.; Shouman, S. A. Targeting
806 colorectal cancer cell metabolism through development of cisplatin and metformin nano-
807 cubosomes. *BMC Cancer* **2018,** *18* (1), 822, DOI: 10.1186/s12885-018-4727-5.
808 (18) Ha, S.; La, Y.; Kim, K. T. Polymer Cubosomes: Infinite Cubic Mazes and Possibilities.
809 *Accounts of Chemical Research* **2020,** *53* (3), 620-631, DOI: 10.1021/acs.accounts.9b00563.
810 (19) He, H.; Rahimi, K.; Zhong, M.; Mourran, A.; Luebke, D. R.; Nulwala, H. B.; Möller, M.;
811 Matyjaszewski, K. Cubosomes from hierarchical self-assembly of poly(ionic liquid) block
812 copolymers. *Nat Commun* **2017,** *8* (1), 14057, DOI: 10.1038/ncomms14057.
813 (20) Aleandri, S.; Bandera, D.; Mezzenga, R.; Landau, E. M. Biotinylated Cubosomes: A
814 Versatile Tool for Active Targeting and Codelivery of Paclitaxel and a Fluorescein-Based Lipid
815 Dye. *Langmuir* **2015,** *31* (46), 12770-12776, DOI: 10.1021/acs.langmuir.5b03469.

816 (21) Caltagirone, C.; Falchi, A. M.; Lampis, S.; Lippolis, V.; Meli, V.; Monduzzi, M.; Prodi, L.;
817 Schmidt, J.; Sgarzi, M.; Talmon, Y.; Bizzarri, R.; Murgia, S. Cancer-Cell-Targeted Theranostic
818 Cubosomes. *Langmuir* **2014,** *30* (21), 6228-6236, DOI: 10.1021/la501332u.
819 (22) Zhai, J.; Luwor, R. B.; Ahmed, N.; Escalona, R.; Tan, F. H.; Fong, C.; Ratcliffe, J.; Scoble,
820 J. A.; Drummond, C. J.; Tran, N. Paclitaxel-Loaded Self-Assembled Lipid Nanoparticles as
821 Targeted Drug Delivery Systems for the Treatment of Aggressive Ovarian Cancer. *ACS Applied*
822 *Materials & Interfaces* **2018,** *10* (30), 25174-25185, DOI: 10.1021/acsami.8b08125.
823 (23) Alcaraz, N.; Liu, Q.; Hanssen, E.; Johnston, A.; Boyd, B. J. Clickable Cubosomes for
824 Antibody-Free Drug Targeting and Imaging Applications. *Bioconjugate Chemistry* **2018,** *29* (1),
825 149-157, DOI: 10.1021/acs.bioconjchem.7b00659.
826 (24) Sagnella, S. M.; Gong, X.; Moghaddam, M. J.; Conn, C. E.; Kimpton, K.; Waddington, L.
827 J.; Krodkiewska, I.; Drummond, C. J. Nanostructured nanoparticles of self-assembled lipid pro-
828 drugs as a route to improved chemotherapeutic agents. *Nanoscale* **2011,** *3* (3), 919-924, DOI:
829 10.1039/c0nr00781a.
830 (25) Biffi, S.; Andolfi, L.; Caltagirone, C.; Garrovo, C.; Falchi, A. M.; Lippolis, V.; Lorenzon,
831 A.; Macor, P.; Meli, V.; Monduzzi, M.; Obiols-Rabasa, M.; Petrizza, L.; Prodi, L.; Rosa, A.;
832 Schmidt, J.; Talmon, Y.; Murgia, S. Cubosomes forin vivofluorescence lifetime imaging.
833 *Nanotechnology* **2016,** *28* (5), 055102, DOI: 10.1088/1361-6528/28/5/055102.
834 (26) Xu, X.; Zhang, X.; Wei, C.; Zheng, D.; Lu, X.; Yang, Y.; Luo, A.; Zhang, K.; Duan, X.;
835 Wang, Y. Targeting SLC7A11 specifically suppresses the progression of colorectal cancer stem
836 cells via inducing ferroptosis. *European Journal of Pharmaceutical Sciences* **2020,** *152*, 105450,
837 DOI: https://doi.org/10.1016/j.ejps.2020.105450.
838 (27) Tiernan, J. P.; Perry, S. L.; Verghese, E. T.; West, N. P.; Yeluri, S.; Jayne, D. G.; Hughes,
839 T. A. Carcinoembryonic antigen is the preferred biomarker for in vivo colorectal cancer
840 targeting. *British journal of cancer* **2013,** *108* (3), 662-667, DOI: 10.1038/bjc.2012.605.
841 (28) Tiernan, J. P.; Ingram, N.; Marston, G.; Perry, S. L.; Rushworth, J. V.; Coletta, P. L.;
842 Millner, P. A.; Jayne, D. G.; Hughes, T. A. CEA-targeted nanoparticles allow specific in vivo
843 fluorescent imaging of colorectal cancer models. *Nanomedicine (Lond)* **2015,** *10* (8), 1223-31,
844 DOI: 10.2217/nnm.14.202 [doi].
845 (29) Ruigrok, Vincent J. B.; Levisson, M.; Eppink, Michel H. M.; Smidt, H.; van der Oost, J.
846 Alternative affinity tools: more attractive than antibodies? *Biochemical Journal* **2011,** *436* (1), 1-
847 13, DOI: 10.1042/bj20101860.
848 (30) Haurum, J. S. Recombinant polyclonal antibodies: the next generation of antibody
849 therapeutics? *Drug Discovery Today* **2006,** *11* (13), 655-660, DOI:
850 https://doi.org/10.1016/j.drudis.2006.05.009.
851 (31) Kyle, S. Affimer Proteins: Theranostics of the Future? *Trends in Biochemical Sciences*
852 **2018,** *43* (4), 230-232, DOI: https://doi.org/10.1016/j.tibs.2018.03.001.
853 (32) Tiede, C.; Tang, A. A. S.; Deacon, S. E.; Mandal, U.; Nettleship, J. E.; Owen, R. L.;
854 George, S. E.; Harrison, D. J.; Owens, R. J.; Tomlinson, D. C.; McPherson, M. J. Adhiron: a
855 stable and versatile peptide display scaffold for molecular recognition applications. *Protein Eng*
856 *Des Sel* **2014,** *27* (5), 145-155, DOI: 10.1093/protein/gzu007.
857 (33) Tiede, C.; Bedford, R.; Heseltine, S. J.; Smith, G.; Wijetunga, I.; Ross, R.; AlQallaf, D.;
858 Roberts, A. P.; Balls, A.; Curd, A.; Hughes, R. E.; Martin, H.; Needham, S. R.; Zanetti-
859 Domingues, L. C.; Sadigh, Y.; Peacock, T. P.; Tang, A. A.; Gibson, N.; Kyle, H.; Platt, G. W.;
860 Ingram, N.; Taylor, T.; Coletta, L. P.; Manfield, I.; Knowles, M.; Bell, S.; Esteves, F.; Maqbool,
861 A.; Prasad, R. K.; Drinkhill, M.; Bon, R. S.; Patel, V.; Goodchild, S. A.; Martin-Fernandez, M.;

Owens, R. J.; Nettleship, J. E.; Webb, M. E.; Harrison, M.; Lippiat, J. D.; Ponnambalam, S.; Peckham, M.; Smith, A.; Ferrigno, P. K.; Johnson, M.; McPherson, M. J.; Tomlinson, D. C. Affimer proteins are versatile and renewable affinity reagents. *Elife* **2017,** *6*, DOI: 10.7554/eLife.24903 [doi].

(34) Michel, M. A.; Swatek, K. N.; Hospenthal, M. K.; Komander, D. Ubiquitin Linkage-Specific Affimers Reveal Insights into K6-Linked Ubiquitin Signaling. *Molecular Cell* **2017,** *68* (1), 233-246.e5, DOI: https://doi.org/10.1016/j.molcel.2017.08.020.

(35) Shamsuddin, S. H.; Jayne, D. G.; Tomlinson, D. C.; McPherson, M. J.; Millner, P. A. Selection and characterisation of Affimers specific for CEA recognition. *Scientific Reports* **2021,** *11* (1), 744, DOI: 10.1038/s41598-020-80354-6.

(36) Shamsuddin, S. H.; Gibson, T. D.; Tomlinson, D. C.; McPherson, M. J.; Jayne, D. G.; Millner, P. A. Reagentless Affimer- and antibody-based impedimetric biosensors for CEA-detection using a novel non-conducting polymer. *Biosensors and Bioelectronics* **2021,** *178*, 113013, DOI: https://doi.org/10.1016/j.bios.2021.113013.

(37) Krasnovskaya, O.; Naumov, A.; Guk, D.; Gorelkin, P.; Erofeev, A.; Beloglazkina, E.; Majouga, A. Copper Coordination Compounds as Biologically Active Agents. *Int J Mol Sci* **2020,** *21* (11), DOI: 10.3390/ijms21113965.

(38) Pramanik, A.; Laha, D.; Dash, S. K.; Chattopadhyay, S.; Roy, S.; Das, D. K.; Pramanik, P.; Karmakar, P. An in-vivo study for targeted delivery of copper-organic complex to breast cancer using chitosan polymer nanoparticles. *Materials Science and Engineering: C* **2016,** *68*, 327-337, DOI: https://doi.org/10.1016/j.msec.2016.05.014.

(39) Pramanik, A.; Laha, D.; Pramanik, P.; Karmakar, P. A novel drug "copper acetylacetonate" loaded in folic acid-tagged chitosan nanoparticle for efficient cancer cell targeting. *Journal of drug targeting* **2013,** *22*, DOI: 10.3109/1061186x.2013.832768.

(40) Jia, Y.-Y.; Zhang, J.-J.; Zhang, Y.-X.; Wang, W.; Li, C.; Zhou, S.-Y.; Zhang, B.-L. Construction of redox-responsive tumor targeted cisplatin nano-delivery system for effective cancer chemotherapy. *International Journal of Pharmaceutics* **2020,** *580*, 119190, DOI: https://doi.org/10.1016/j.ijpharm.2020.119190.

(41) Peng, J. Q.; Fumoto, S.; Suga, T.; Miyamoto, H.; Kuroda, N.; Kawakami, S.; Nishida, K. Targeted co-delivery of protein and drug to a tumor in vivo by sophisticated RGD-modified lipid-calcium carbonate nanoparticles. *Journal of Controlled Release* **2019,** *302*, 42-53, DOI: https://doi.org/10.1016/j.jconrel.2019.03.021.

(42) Sykes, E. A.; Chen, J.; Zheng, G.; Chan, W. C. W. Investigating the Impact of Nanoparticle Size on Active and Passive Tumor Targeting Efficiency. *ACS Nano* **2014,** *8* (6), 5696-5706, DOI: 10.1021/nn500299p.

(43) Tang, L.; Yang, X.; Yin, Q.; Cai, K.; Wang, H.; Chaudhury, I.; Yao, C.; Zhou, Q.; Kwon, M.; Hartman, J. A.; Dobrucki, I. T.; Dobrucki, L. W.; Borst, L. B.; Lezmi, S.; Helferich, W. G.; Ferguson, A. L.; Fan, T. M.; Cheng, J. Investigating the optimal size of anticancer nanomedicine. *Proceedings of the National Academy of Sciences* **2014,** *111* (43), 15344, DOI: 10.1073/pnas.1411499111.

(44) Tan, C.-P.; Lu, Y.-Y.; Ji, L.-N.; Mao, Z.-W. Metallomics insights into the programmed cell death induced by metal-based anticancer compounds. *Metallomics* **2014,** *6* (5), 978-995, DOI: 10.1039/c3mt00225j.

(45) Bazylińska, U.; Kulbacka, J.; Schmidt, J.; Talmon, Y.; Murgia, S. Polymer-free cubosomes for simultaneous bioimaging and photodynamic action of photosensitizers in melanoma skin

907 cancer cells. *Journal of Colloid and Interface Science* **2018,** *522*, 163-173, DOI:
908 https://doi.org/10.1016/j.jcis.2018.03.063.
909 (46) Kulkarni, C. V.; Tang, T.-Y.; Seddon, A. M.; Seddon, J. M.; Ces, O.; Templer, R. H.
910 Engineering bicontinuous cubic structures at the nanoscale—the role of chain splay. *Soft Matter*
911 **2010,** *6* (14), 3191-3194, DOI: 10.1039/c0sm00068j.
912 (47) Jason, B.; Hesson, C.; Martin, C. The Temperature-Composition Phase Diagram and
913 Mesophase Structure Characterization of the Monoolein/Water System. *J. Phys. II France* **1996,**
914 *6* (5), 723-751.
915 (48) Barauskas, J.; Johnsson, M.; Joabsson, F.; Tiberg, F. Cubic Phase Nanoparticles
916 (Cubosome): Principles for Controlling Size, Structure, and Stability. *Langmuir* **2005,** *21* (6),
917 2569-2577, DOI: 10.1021/la047590p.
918 (49) Sagalowicz, L.; Michel, M.; Adrian, M.; Frossard, P.; Rouvet, M.; Watzke, H. J.; Yaghmur,
919 A.; De Campo, L.; Glatter, O.; Leser, M. E. Crystallography of dispersed liquid crystalline
920 phases studied by cryo-transmission electron microscopy. *Journal of Microscopy* **2006,** *221* (2),
921 110-121, DOI: https://doi.org/10.1111/j.1365-2818.2006.01544.x.
922 (50) Grunnet, M.; Sorensen, J. B. Carcinoembryonic antigen (CEA) as tumor marker in lung
923 cancer. *Lung Cancer* **2012,** *76* (2), 138-143, DOI: 10.1016/j.lungcan.2011.11.012.
924 (51) Kaushal, S.; McElroy, M. K.; Luiken, G. A.; Talamini, M. A.; Moossa, A. R.; Hoffman, R.
925 M.; Bouvet, M. Fluorophore-conjugated anti-CEA antibody for the intraoperative imaging of
926 pancreatic and colorectal cancer. *J Gastrointest Surg* **2008,** *12* (11), 1938-1950, DOI:
927 10.1007/s11605-008-0581-0.
928 (52) Lázaro-Gorines, R.; Ruiz-de-la-Herrán, J.; Navarro, R.; Sanz, L.; Álvarez-Vallina, L.;
929 Martínez-del-Pozo, A.; Gavilanes, J. G.; Lacadena, J. A novel Carcinoembryonic Antigen
930 (CEA)-Targeted Trimeric Immunotoxin shows significantly enhanced Antitumor Activity in
931 Human Colorectal Cancer Xenografts. *Scientific Reports* **2019,** *9* (1), 11680, DOI:
932 10.1038/s41598-019-48285-z.
933 (53) Hama, S.; Itakura, S.; Nakai, M.; Nakayama, K.; Morimoto, S.; Suzuki, S.; Kogure, K.
934 Overcoming the polyethylene glycol dilemma via pathological environment-sensitive change of
935 the surface property of nanoparticles for cellular entry. *Journal of Controlled Release* **2015,** *206*,
936 67-74, DOI: https://doi.org/10.1016/j.jconrel.2015.03.011.
937 (54) Lee, J. M.; Choi, J. W.; Ahrberg, C. D.; Choi, H. W.; Ha, J. H.; Mun, S. G.; Mo, S. J.;
938 Chung, B. G. Generation of tumor spheroids using a droplet-based microfluidic device for
939 photothermal therapy. *Microsystems & Nanoengineering* **2020,** *6* (1), 52, DOI: 10.1038/s41378-
940 020-0167-x.
941 (55) Costa, E. C.; Moreira, A. F.; de Melo-Diogo, D.; Gaspar, V. M.; Carvalho, M. P.; Correia, I.
942 J. 3D tumor spheroids: an overview on the tools and techniques used for their analysis.
943 *Biotechnology Advances* **2016,** *34* (8), 1427-1441, DOI:
944 https://doi.org/10.1016/j.biotechadv.2016.11.002.
945 (56) Loessner, D.; Stok, K. S.; Lutolf, M. P.; Hutmacher, D. W.; Clements, J. A.; Rizzi, S. C.
946 Bioengineered 3D platform to explore cell–ECM interactions and drug resistance of epithelial
947 ovarian cancer cells. *Biomaterials* **2010,** *31* (32), 8494-8506, DOI:
948 https://doi.org/10.1016/j.biomaterials.2010.07.064.
949 (57) Ireson, C. R.; Alavijeh, M. S.; Palmer, A. M.; Fowler, E. R.; Jones, H. J. The role of mouse
950 tumour models in the discovery and development of anticancer drugs. *British Journal of Cancer*
951 **2019,** *121* (2), 101-108, DOI: 10.1038/s41416-019-0495-5.

952 (58) Prange, J. A.; Aleandri, S.; Komisarski, M.; Luciani, A.; Käch, A.; Schuh, C.-D.; Hall, A.
953 M.; Mezzenga, R.; Devuyst, O.; Landau, E. M. Overcoming Endocytosis Deficiency by
954 Cubosome Nanocarriers. *ACS Applied Bio Materials* **2019,** *2* (6), 2490-2499, DOI:
955 10.1021/acsabm.9b00187.
956 (59) Haute, D. V.; Berlin, J. M. Challenges in realizing selectivity for nanoparticle
957 biodistribution and clearance: lessons from gold nanoparticles. *Therapeutic Delivery* **2017,** *8* (9),
958 763-774, DOI: 10.4155/tde-2017-0057.
959 (60) De Jong, W. H.; Hagens, W. I.; Krystek, P.; Burger, M. C.; Sips, A. J. A. M.; Geertsma, R.
960 E. Particle size-dependent organ distribution of gold nanoparticles after intravenous
961 administration. *Biomaterials* **2008,** *29* (12), 1912-1919, DOI:
962 https://doi.org/10.1016/j.biomaterials.2007.12.037.
963 (61) Li, S.; Zhang, J.; Deng, C.; Meng, F.; Yu, L.; Zhong, Z. Redox-Sensitive and Intrinsically
964 Fluorescent Photoclick Hyaluronic Acid Nanogels for Traceable and Targeted Delivery of
965 Cytochrome c to Breast Tumor in Mice. *ACS Applied Materials & Interfaces* **2016,** *8* (33),
966 21155-21162, DOI: 10.1021/acsami.6b05775.
967 (62) Izci, M.; Maksoudian, C.; Manshian, B. B.; Soenen, S. J. The Use of Alternative Strategies
968 for Enhanced Nanoparticle Delivery to Solid Tumors. *Chemical Reviews* **2021,** *121* (3), 1746-
969 1803, DOI: 10.1021/acs.chemrev.0c00779.
970 (63) Feng, H.-Y.; Yuan, Y.; Zhang, Y.; Liu, H.-J.; Dong, X.; Yang, S.-C.; Liu, X.-L.; Lai, X.;
971 Zhu, M.-H.; Wang, J.; Lu, Q.; Lin, Q.; Chen, H.-Z.; Lovell, J. F.; Sun, P.; Fang, C. Targeted
972 Micellar Phthalocyanine for Lymph Node Metastasis Homing and Photothermal Therapy in an
973 Orthotopic Colorectal Tumor Model. *Nano-Micro Letters* **2021,** *13* (1), 145, DOI:
974 10.1007/s40820-021-00666-8.
975 (64) Wei, Y.; Gu, X.; Sun, Y.; Meng, F.; Storm, G.; Zhong, Z. Transferrin-binding peptide
976 functionalized polymersomes mediate targeted doxorubicin delivery to colorectal cancer in vivo.
977 *Journal of controlled release : official journal of the Controlled Release Society* **2020,** *319*, 407-
978 415, DOI: 10.1016/j.jconrel.2020.01.012.
979 (65) Esteban-Fernández, D.; Verdaguer, J. M.; Ramírez-Camacho, R.; Palacios, M. A.; Gómez-
980 Gómez, M. M. Accumulation, Fractionation, and Analysis of Platinum in Toxicologically
981 Affected Tissues after Cisplatin, Oxaliplatin, and Carboplatin Administration. *Journal of
982 Analytical Toxicology* **2008,** *32* (2), 140-146, DOI: 10.1093/jat/32.2.140.
983 (66) Wei, Y.; Gu, X.; Sun, Y.; Meng, F.; Storm, G.; Zhong, Z. Transferrin-binding peptide
984 functionalized polymersomes mediate targeted doxorubicin delivery to colorectal cancer in vivo.
985 *Journal of Controlled Release* **2020,** *319*, 407-415, DOI:
986 https://doi.org/10.1016/j.jconrel.2020.01.012.
987 (67) M. Basham; J. Filik; M.T. Wharmby; al., P. C. C. e. Data Analysis WorkbeNch (DAWN).
988 *Journal of Synchrotron Radiation* **2015,** *22* (3), 853-8.
989 (68) Filik, J.; Ashton, A. W.; Chang, P. C. Y.; Chater, P. A.; Day, S. J.; Drakopoulos, M.;
990 Gerring, M. W.; Hart, M. L.; Magdysyuk, O. V.; Michalik, S.; Smith, A.; Tang, C. C.; Terrill, N.
991 J.; Wharmby, M. T.; Wilhelm, H. Processing two-dimensional X-ray diffraction and small-angle
992 scattering data in DAWN 2. *J Appl Crystallogr* **2017,** *50* (Pt 3), 959-966, DOI:
993 10.1107/s1600576717004708.
994 (69) Tinevez, J.-Y.; Perry, N.; Schindelin, J.; Hoopes, G. M.; Reynolds, G. D.; Laplantine, E.;
995 Bednarek, S. Y.; Shorte, S. L.; Eliceiri, K. W. TrackMate: An open and extensible platform for
996 single-particle tracking. *Methods* **2017,** *115*, 80-90, DOI:
997 https://doi.org/10.1016/j.ymeth.2016.09.016.

998 (70) Ingram, N.; Macnab, S. A.; Marston, G.; Scott, N.; Carr, I. M.; Markham, A. F.;
999 Whitehouse, A.; Coletta, P. L. The use of high-frequency ultrasound imaging and
1000 biofluorescence for in vivo evaluation of gene therapy vectors. *BMC Med Imaging* **2013,** *13*, 35,
1001 DOI: 1471-2342-13-35 [pii]

1002 10.1186/1471-2342-13-35 [doi].

1003